Progress in Oceanography 220 (2024) 103174

Contents lists available at ScienceDirect

Progress in Oceanography

journal homepage: www.elsevier.com/locate/pocean

From winter to late summer in the northwestern Barents Sea shelf: Impacts of seasonal progression of sea ice and upper ocean on nutrient and phytoplankton dynamics

Zoe Koenig [a,b,c,*], Morven Muilwijk [b], Håkon Sandven [b,d], Øyvind Lundesgaard [b], Philipp Assmy [b], Sigrid Lind [b], Karen M. Assmann [e], Melissa Chierici [e], Agneta Fransson [b], Sebastian Gerland [b], Elizabeth Jones [e], Angelika H.H. Renner [e], Mats A. Granskog [b]

[a] UiT The Arctic University of Norway, Tromsø, Norway
[b] Norwegian Polar Institute, Fram Centre, Tromsø, Norway
[c] Geophysical Institute and Bjerknes Center for Climate Research, The University of Bergen, Bergen, Norway
[d] Department of Physics and Technology, University of Bergen, Bergen, Norway
[e] Institute of Marine Research, Fram Centre, Tromsø, Norway

ARTICLE INFO

Keywords:
Seasonal changes
Sea ice
Hydrography
Nutrients (mineral)
Phytoplankton
Barents Sea

ABSTRACT

Strong seasonality is a key feature of high-latitude systems like the Barents Sea. While the interannual variability and long-term changes of the Barents Sea are well-documented, the seasonal progression of the physical and biological systems is less known, mainly due to poor accessibility of the seasonally ice-covered area in winter and spring. Here, we use an extensive set of physical and biological *in situ* observations from four scientific expeditions covering the seasonal progression from late winter to late summer 2021 in the northwestern Barents Sea, from fully ice-covered to ice-free conditions. We found that sea ice meltwater and the timing of ice-free conditions in summer shape the environment, controlling heat accumulation, light and nutrient availability, and biological activity vertically, seasonally, and meridionally. In March and May, the ocean north of the Polar Front was ice-covered and featured a deep mixed layer. Chlorophyll-*a* concentrations increased strongly from March to May along with greater euphotic depth, indicating the beginning of the spring bloom despite the absence of surface layer stratification. By July and in September, sea ice meltwater created a shallow low-density surface layer that strengthened stratification. In open water, chlorophyll-*a* maxima were found at the base of this layer as surface nutrients were depleted, while in the presence of ice, maxima were closer to the surface. Solar heating and the thickness of the surface layer increased with the number of ice-free days. The summer data showed a prime example of an Arctic-like space-for-time seasonal variability in the key physical and biological patterns, with the summer situation progressing northwards following sea ice retreat. The amount of sea ice melt (local or imported) has a strong control on the conditions in the northwestern Barents Sea, and the conditions in late 2021 resembled pre-2010 Arctic-like conditions with high freshwater content and lower ocean heat content.

1. Introduction

The northern Barents Sea is a hotspot of Arctic climate change with the largest winter sea ice loss observed Arctic-wide (Onarheim et al., 2018) and an atmospheric warming of 2–2.5 times the Arctic average and 5–7 times the global average (Isaksen et al., 2022), which also extends to the ocean (Lind and Ingvaldsen, 2012; Smedsrud et al., 2013; Lind et al., 2018; Ingvaldsen et al., 2021; Smedsrud et al., 2022). Although the Barents Sea is among the most extensively studied areas of the Arctic Ocean, observations from autumn, winter, and spring are sparse and sporadic, especially in the ice-covered northern part. While extreme seasonality is a characteristic of high-latitude systems (e.g. Leu et al., 2015), the seasonal development of the northwestern Barents Sea shelf is not well known, in contrast to the well documented long-term climatic changes and interannual variability. In the southern regions of the Barents Sea, there has been more extensive research into

* Corresponding author.
E-mail address: zoe.c.koenig@uit.no (Z. Koenig).

https://doi.org/10.1016/j.pocean.2023.103174

Available online 22 November 2023

seasonality. For instance, the seasonal inflow of warm Atlantic water has been monitored (Ingvaldsen et al., 2004), and studies have delved into the seasonal fluxes of particulate biogenic matter (Olli et al., 2002) and CO_2 (Omar et al., 2007) within the marginal ice zone. Investigations into the seasonal variations in the distribution of phyto- and proto-zooplankton have also been conducted (e.g. Rat'kova and Wassmann, 2002; Riser et al., 2002; Arashkevich et al., 2002), along with explorations of higher trophic levels such as fish (Eriksen et al., 2021). Additionally, research has examined the seasonality of the sea ice cover, utilizing satellite data (Onarheim et al., 2018) and models (Koenigk et al., 2009). Insights into seasonal oceanic variability have been drawn from reanalysis efforts (Smedsrud et al., 2013) and models (Sandø et al., 2010). Despite these endeavors, there remains a notable research gap pertaining to the understanding of how the physical environment transforms from winter to summer and the interplay of this transformation with biological patterns, especially in the northern Barents Sea with limited observational studies.

In this paper, we describe the seasonal progression of the seasonally ice-covered northwestern Barents Sea shelf (Fig. 1b) from late winter to late summer 2021, observed during four research expeditions along a south-to-north transect. These unique data show how the seasonal changes in sea ice and the upper ocean shape the conditions for phytoplankton growth, primarily through the retreat and melt of sea ice and the build-up of stratification, which impact light and nutrient availability. We demonstrate how seasonality is a fundamental characteristic of this high latitude marine system and a crucial aspect to consider in the context of changing long-term trends.

The long-term trends in the physical environment of the Barents Sea, commonly referred to as Atlantification (Årthun et al., 2012; Polyakov et al., 2017), have cascading effects on the Barents Sea marine

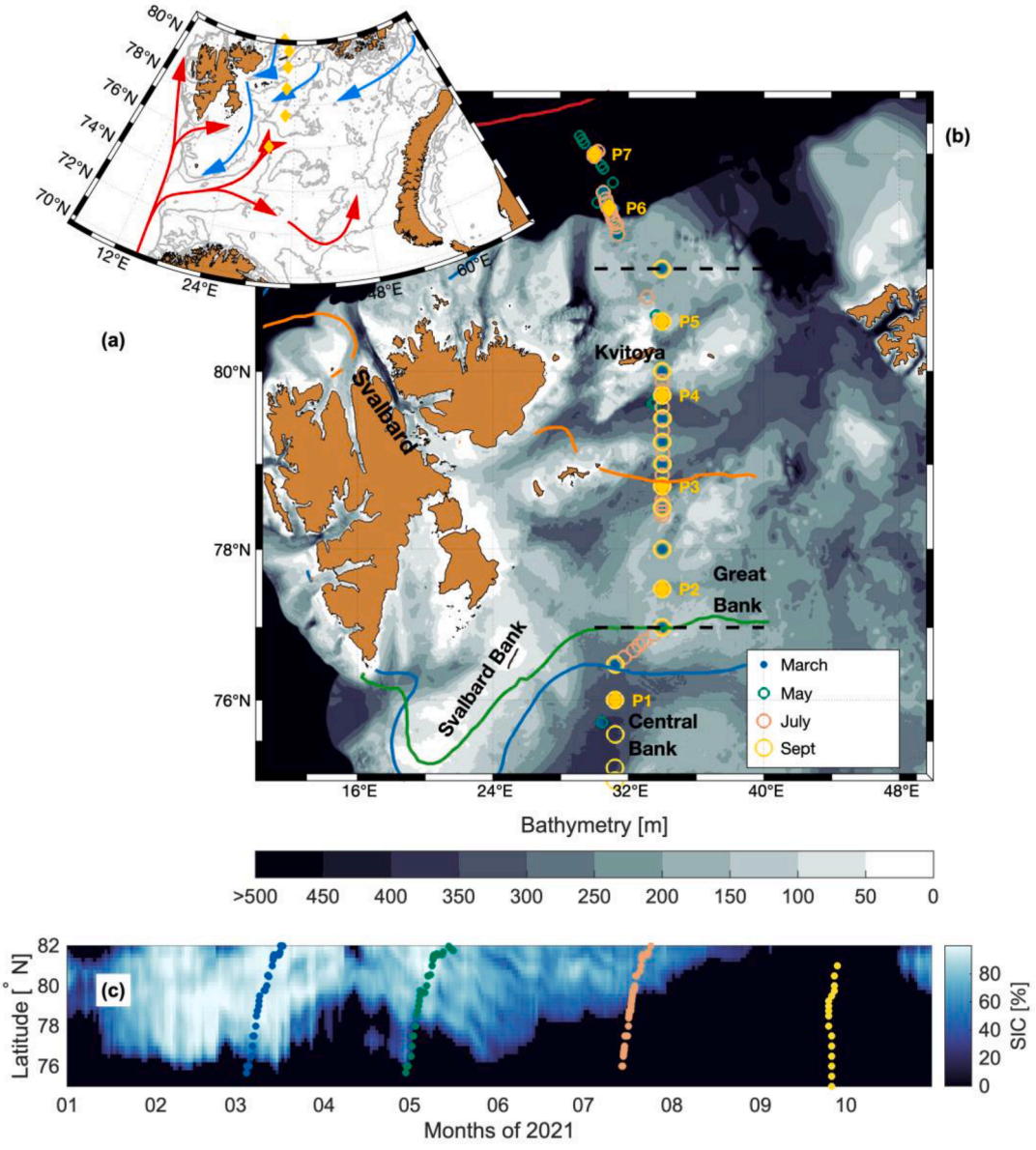

Fig. 1. a) Main ocean circulation patterns in the Barents Sea. The red arrows illustrate the Atlantic Water branches and the blue arrows illustrate the surface Polar Water flow. Background is the bathymetry. b) Close-up of the sampling transect. The main P-stations are indicated on the map with yellow diamonds. All the CTD stations for the different cruises are indicated by circles: March in blue, May in green, July in orange, and September in yellow. The bathymetry is from IBCAO-v3 (Jakobsson et al., 2012). The thick solid lines are the mean sea ice edge for March (blue), May (green), July (orange), and September (red). The black dashed lines indicate the focus area between 77 and 81°N on the northwestern Barents Sea Shelf. c) Hovmöller diagram of daily sea ice concentration (SIC) along the transects in 2021. The blue, green, orange, and yellow dots are the CTD stations in March, May, July, and September, respectively.

ecosystem, including increased pelagic primary production (Arrigo and van Dijken, 2015; Dalpadado et al., 2020), northward expansion of boreal species (Berge et al., 2015; Fossheim et al., 2015; Paulsen et al., 2016; Lefort et al., 2020; Oziel et al., 2020), and the increased importance of the pelagic ecosystem at the expense of ice-associated and benthic ecosystems (Ingvaldsen et al., 2021). Atlantification directly impacts phytoplankton, driving significant ecosystem changes (Siwertsson et al., 2023), with the most pronounced effects observed in the northeastern Barents Sea, leading to the strongest Arctic-wide increase in net primary production (Frey et al., 2021). However, it is worth noting that models and satellite observations show no clear trend in primary production for the northwestern part (Castro de la Guardia et al., 2023).

Alongside Atlantification, the Barents Sea experienced a 40 % decrease in freshwater input from sea ice melt from 1970 to 1999 (Lind et al., 2018), leading to a transition from a cold and stratified Arctic-like surface regime to a warmer, well-mixed Atlantic-dominated regime (Lind et al., 2018; Polyakov et al., 2020), with projected continuation of this trend (Muilwijk et al., 2023). A more mixed regime impacts light availability for primary producers (Petit et al., 2022), and may favor an influx of nutrients into the surface layer (Jones et al., 2023; Randelhoff et al., 2016; Renner et al., 2023), which drives the increase in primary production, a scenario supported by remote sensing (Kahru et al., 2016; Lewis et al., 2020).

Observations, satellite data, and previous modeling studies have identified the inflow of sea ice from the Central Arctic Ocean and the inflow of Atlantic Water as the two primary factors influencing freshwater/stratification and local sea ice cover in the northern Barents Sea (Ellingsen et al., 2009; Koenigk et al., 2009; Lind et al., 2018; Aaboe et al., 2021; Efstathiou et al., 2022; Lundesgaard et al., 2022; Hordoir et al., 2022). Since hydrographic monitoring began in the 1970's, the seasonal surface layer has been observed every summer as a less-dense layer in the upper 20–30 m in the northern Barents Sea, forming from a varying amount of freshwater input and warming due to surface heat fluxes (longwave and shortwave radiation; Loeng, 1991; Pfirman et al., 1994; Lind and Ingvaldsen, 2012; Lind et al., 2016, 2018; Petit et al., 2022). Lagged correlation analyses indicate that the summer meltwater input is mixed down to ~ 100 m depth with a one-year lag over the period 1970–2016 (Lind et al., 2018). Since the mid-2000s, a decline in sea ice inflow led to a major reduction of ocean freshwater content and weakened ocean stratification, allowing for more vertical mixing and rapid upper ocean warming in the northern Barents Sea (Lind et al., 2018). However, the substantial sea ice inflow in 2019 partly reversed this trend (Aaboe et al., 2021; Lundesgaard et al., 2022).

Between the late 1990s and the early 2000s, primary production in the northern Barents Sea was primarily influenced by the open water fraction and length of the growing season. With the region now being ice-free or only partly ice-covered during summer, nutrient availability has emerged as the main driver since 2009 (Lewis et al., 2020). A shift from a light-limited to a nutrient-limited system (Babin, 2020) is likely to impact the timing, magnitude, and fate of primary production with potential cascading effects on higher trophic levels, but we lack a good understanding of how these processes unfold over seasonal timescales. In the case of a longer meltwater-stratified open water period, this is likely to extend the oligotrophic summer season dominated by small-sized phytoplankton, which is not the preferred food for the large Arctic zooplankton grazers (Kohlbach et al., 2023). This hypothesis agrees with findings from Fram Strait that showed a reduced biological carbon pump as a result of increased meltwater stratification (von Appen et al., 2021). However, how the balance between buoyancy fluxes and vertical mixing plays out at the ecosystem level is poorly known, especially seasonally. In the following, we examine the evolution of the physical environment in the northwestern Barents Sea from late winter to late summer 2021 and how it shapes phytoplankton phenology and nutrient concentration.

2. Material and methods

2.1. In situ data

We used hydrographic, sea ice, nutrient, and chlorophyll-*a* data from four scientific cruises, approximately two months apart, in the northwestern Barents Sea between March and September 2021. The Nansen Legacy cruises Q1 in late winter (2–25 March, Gerland et al., 2022), Q2 in spring (27 April to 20 May, Ludvigsen et al., 2022), and JC2-1 in summer (12–29 July, Jones et al., 2022a) with *R/V Kronprins Haakon* were multidisciplinary and sampled a large set of physical, chemical and biological variables. The transect followed the 30°E longitude from south to north and consisted of 24-hour process stations (so-called P-stations) and additional CTD stations with sampling for chemistry (Fig. 1b). The fourth survey was performed as part of an ecosystem cruise in late summer by the Institute of Marine Research from 25 to 28 September with *R/V Hellmer Hanssen* and *R/V Johan Hjort* (Vardø North (VN) transect). Hereafter, we will refer to the cruises based on their month: March (Q1, late winter), May (Q2, spring), July (JC2-1, summer), and September (VN, late summer).

We divided the south-to-north transect, covered by all cruises, into three parts (dashed black lines in Fig. 1b). Our emphasis in this study is on the middle part of the transect to examine the seasonal development of the northwestern Barents Sea shelf, north of the average location of the Polar Front (Loeng, 1991; Barton et al., 2018) and south of the shelf break (i.e., from 77 to 81°N). This focus area is typically fully ice-covered during winter, while it becomes ice-free by late summer, and exhibits the most Arctic-like conditions. The focus area is distinctly different from the southern part of the section, where there is an Atlantic Ocean climate, and from the northern shelf-slope region, where the Atlantic Water Boundary Current dominates, and conditions are highly impacted by advection rather than local processes (Renner et al., 2018).

2.1.1. Water column data for the first three cruises: March, May, and July

2.1.1.1. CTD sensor. Water column hydrography was investigated using vertical profiles of temperature and salinity obtained with a conductivity-temperature-depth (CTD, SBE-911 plus, Sea-bird Scientific) sensor mounted on a rosette equipped with 24 Niskin bottles used for seawater sampling. Pressure, temperature, and practical salinity data from the CTD are accurate to ± 0.5 dbar, $\pm 10^{-3}$ °C, and $\pm 3 \times 10^{-3}$, respectively. CTD data were processed using the standard SBE Data Processing software. We used the International Thermodynamic Equations of Seawater (TEOS-10) (McDougall and Barker, 2011) to convert temperature and practical salinity to Conservative Temperature (Θ) and Absolute Salinity (S_A). The CTD datasets corresponding to the three first cruises (March, May, and July) are available from Gerland (2022), Ludvigsen (2022), and Jones (2022).

2.1.1.2. Chlorophyll-a and beam attenuation. The CTD was equipped with an additional factory-calibrated sensor for chlorophyll-*a* fluorescence (WET Labs ECO fluorometer). The *in situ* chlorophyll-*a* fluorometer measurements ($[chl]_{con}$) were corrected using laboratory measurements of chlorophyll-*a* concentrations ($[chl]_{meas}$) from filtered water samples (Vader, 2022), which were used to develop a linear relationship with the *in situ* fluorescence. Here, seasonal relationships had to be developed (Sandven et al., 2023) due to physiological and species variability in phytoplankton, which is well-known to cause large temporal and regional biases in fluorescence measurements (Roesler et al., 2017). For the March and May cruise, we used the relationship $[chl]_{con} = 1.1137 \cdot [chl]_{meas} - 0.009$, while for the July cruise, the relationship $[chl]_{con} = 0.6752 \cdot [chl]_{meas} - 0.006$ was used to correct the fluorescence measurements. Over the entire data set, the root-mean square error was 0.47 mg m^{-3} (NRSMD = 7.63 %, R^2 = 0.78) when comparing the corrected chlorophyll-*a* fluorescence measurements with

the water sample chlorophyll-*a* concentrations. *In situ* chlorophyll-*a* fluorescence (factory calibration) underestimated the water sample chlorophyll-*a* concentration by around 10 % in May, while in July it was overestimated by approximately 50 % (see also Sandven et al., 2023). For global ocean data sets, fluorometers have been found to overestimate chlorophyll-*a* concentrations by around 100 %, with large residual spread in the data (Roesler et al., 2017). While there can be large interspecies variability, other factors such as growth phase, nutrient limitation, grazing, photoacclimation, and non-photochemical quenching may also affect the *in situ* fluorescence. The use of *in situ* fluorescence here may therefore be interpreted as a high-resolution interpolation of the discrete chlorophyll-*a* concentrations measured with water samples, with some additional error sources introduced through the calibration relationship.

Optical beam attenuation was measured using a SeaBird C-Star transmissometer (650 nm, 0.25 m path length). The measured attenuation coefficient was calculated by subtracting the lowest values recorded on each cruise (Sandven et al., 2023), which was made possible by doing deep casts into extremely clear waters in the Nansen Basin on the first three cruises. This procedure has been used in other studies in the Arctic (Neukermans et al., 2014; Gardner et al., 2022), and is described in more detail in the companion article on seasonality of optical properties in the north-western Barents Sea (Sandven et al., 2023).

2.1.1.3. Photosynthetically active radiation (PAR). PAR measurements were collected using a Biospherical QCP-2350-HP sensor. Due to influence from the ship, the PAR data shallower than 41 m were disregarded.

We define an isolume depth for describing the euphotic zone, which is the depth where the PAR is equal to the compensation irradiance. The compensation irradiance is the irradiance at which gains through primary production are balanced by losses from auto- and heterotrophic respiration, grazing, and sinking. However, it is difficult to exactly define the compensation irradiance due to variations in ecophysiological state and phytoplankton species composition affecting the productivity and losses. Siegel et al. (2002) estimated the compensation irradiance in the North Atlantic to be 15 μmol photons m^{-2} s^{-1} (1.3 mol photons m^{-2} day^{-1}), but studies on under-ice blooms have often used lower compensation irradiances, such as 10 μmol photons m^{-2} s^{-1} (Horvat et al., 2022) and 4 μmol photons m^{-2} s^{-1} (Randelhoff et al., 2019). We calculate the isolume depth for 10 μmol photons m^{-2} s^{-1}, estimated from each CTD cast, with the isolumes for other compensation irradiance shown as error bars to illustrate its variability. Isolume depths for compensation irradiance values were calculated using interpolation whenever the isolume depths were deeper than 40 m. Shallower isolume depths were determined from linear extrapolation of log-transformed PAR values. If there is an increase in the diffuse attenuation coefficient, due to for instance higher chlorophyll-*a* concentrations (see Fig. S1), this extrapolation will lead to an underestimate of the isolume, and by contrast an overestimate if there are lower chlorophyll-*a* concentrations near the surface.

In previous studies at lower latitudes, it has been common to convert instantaneous PAR profiles into diurnal integrated values to account for changes in the solar zenith angle throughout the year, see for instance Oziel et al. (2019). This is more challenging at high latitudes, where the sun is close to the horizon for most of the year, such that most radiative transfer models are inaccurate and common relationships for converting instantaneous measurements to daily values no longer hold. In addition, the sea ice cover and cloud conditions strongly influence the diurnal variability, which makes the conversion even more challenging. Using the radiative transfer model accuRT (Stamnes et al., 2018), we consequently found the conversion into daily integrated PAR values to introduce large uncertainties, while not fundamentally changing the large-scale pattern calculated using the instantaneous values. Therefore, we chose to only use instantaneous PAR measurements to estimate the isolume depths, given that the large number of profiles still gives an adequate description of the light environment during each of the cruises.

2.1.1.4. Water Sampling. Water samples were collected at each P-station from the whole water column for inorganic nutrients (nitrate [NO_3^-], nitrite [NO_2^-], phosphate [PO_4^{3-}], and silicic acid [$Si(OH)_4$]). In the following, we will concentrate on nitrate, nitrite, and silicic acid as the main nutrients limiting total and diatom-based production (Tremblay et al., 2015). Unfiltered nutrient samples were sampled into 20 mL vials, preserved with 250 μL chloroform, and stored dark at 4 °C. Post-cruise analysis was performed using a colorimetric method (Grasshoff et al., 1983; Gundersen et al., 2022) at the Institute of Marine Research, Bergen, Norway. The detection limits were 0.5 mmol m^{-3} for [NO_3^-], 0.06 mmol m^{-3} for [PO_4^{3-}] and 0.7 mmol m^{-3} for [$Si(OH)_4$], respectively.

Chlorophyll-*a* samples were taken from Niskin bottles at standard depths (11 to 20 samples depending on water depth), from the surface (5 or 10 m depth) to 10 m above the sea floor at the P-stations. Chlorophyll-*a* samples were filtered through Whatman GF/F filters (nominal pore size 0.7 μm) and extracted directly in 5 mL methanol (>99.9 %) for 12 h at 4 °C in the dark. Chlorophyll-*a* and phaeophytin concentrations in extracts were measured onboard using a Turner 10-AU or Turner Trilogy fluorometer before and after acidification with two drops of 5 % HCl (Holm-Hansen and Riemann, 1978). For further details see the Nansen Legacy sampling protocol (Nansen Legacy protocols, 2022). The nutrient data are available at Jones et al., (2022b-d). The chlorophyll-*a* dataset can be found in Vader, 2022.

2.1.1.5. Deployment procedure of the CTD. The CTD was deployed mainly through R/V *Kronprins Haakon's* moonpool during the March and May cruises due to the extensive presence of sea ice in the study area and relatively low temperatures. The CTD was deployed over the side of the ship during the July cruise. When the moonpool was used, we did not use the uppermost 13 m of the CTD profile. We also took some CTD measurements from the side of the ship at the P-stations during the March and May cruises (Sandven et al., 2023), and these show that there was a homogeneous winter mixed layer from ~ 100 m all the way to the surface, justifying that one may use the uppermost trustworthy data point (at 13 m) and extrapolate up to the surface on the March and May cruises. Since the upper water column was well mixed in March, water samples were only collected from the rosette deployed through the moonpool. During the May cruise, when the phytoplankton spring bloom started to develop, additional chlorophyll-*a* samples from 5 m depth were taken from the side of the ship. During the July cruise, 5 m was added as a standard sampling depth.

2.1.2. Water column data for the September cruise

All but the five northernmost stations on the extended VN section in September 2021 were taken from R/V *Johan Hjort*. Those five northernmost stations were taken from R/V *Helmer Hanssen*. From both ships, water column hydrography was investigated using vertical profiles of temperature and salinity obtained with a CTD (SBE-911 plus) sensor. Pressure, temperature, and practical salinity data from the CTD are accurate to ± 0.5 dbar, $\pm 10^{-3}$ °C, and $\pm 3 \times 10^{-3}$, respectively. Also, for this cruise, the CTD data were processed using the standard SBE Data Processing software. Beam attenuation and chlorophyll-*a* data are not available for September. CTD data from the extended VN section in September 2021 are available on request from datahjelp@imr.no.

2.2. Calculation of physical properties

The heat and freshwater contents were estimated in the upper 100 m from the ocean *in situ* measurements in the four expeditions of 2021, following the procedure in Lind et al. (2018) with a salinity reference of 35 g kg^{-1} and a temperature reference of 0 °C. The mixed layer depth is defined as the depth where the potential density exceeds the surface potential density by 0.03 kg m^{-3} (Cole et al., 2014). As the pycnocline is

relatively strong in the region, the depth of the mixed layer is not sensitive to the method chosen (not shown). The mixing layer refers to the depth to which turbulent mixing, generated by stress at the surface, extends into the water column. This may be different from the mixed layer depth, which continues to exist even after the active mixing diminishes.

The strength of stratification in the water column is quantified using the square of the Brunt–Väisälä buoyancy frequency N, given by $N^2 = -(g/\rho o)\partial\rho/\partial z$, where ρ is the potential density of seawater, ρ_0 is the reference density (1030 kg m^{-3}), and g is the acceleration due to gravity. This parameter provides a detailed profile of the stability of the water column.

We define the nitracline as the maximum gradient in nitrate concentration and use the term nutricline when referring to nutrients in a general context (including phosphate and silicic acid).

2.3. Ancillary data

Daily mean sea ice concentrations (SIC) based on satellite observations at 10 km grid resolution are obtained from the EUMETSAT Ocean and Sea Ice Satellite Application Facility (OSI SAF, https://www.osi-saf.org). This dataset is a product based on passive microwave (DMSP/SSMIS) data. The days of open water before a station are defined as the number of days with sea ice concentration of less than 15 % preceding the day of the occupation of the station. Sea ice drift in the region was taken from NSIDC Polar Pathfinder Daily 25 km EASE-GRID Sea Ice Motion Vectors, version 4.1 (Tschudi et al., 2019). Air temperatures are from observations at the weather station on the island Kvitøya (31.459°E, 80.104°N), located in the northern part of the study area (Fig. 1b), courtesy of MET Norway, freely available from https://api.met.no/.

3. Results

3.1. Atmosphere and sea ice

Air temperatures on the island Kvitøya show that temperatures in the region were below 0 °C from mid-November 2020 until the end of May 2021, hovered around 0 °C in June 2021, and were on average + 1.0 °C in July and August 2021 (not shown). The atmospheric circulation patterns changed between the expeditions, with storms passing in March (not shown), seen as low pressure in the monthly mean sea level pressure, while there was a change to more northerly winds and higher sea level pressure in May (not shown) associated with stronger southward ice drift from the north (Fig. 2).

In March, the entire focus area on the northwestern shelf (77 to 81°N) was ice-covered (Fig. 1c and Fig. 2). Although the sea ice extent was comparable in March and May, sea ice concentration (SIC) was lower in May than in March and had gone through periods with very low SIC between the March and May cruises, especially in the southern part of the transect (Fig. 1c and Fig. 2). By July only the northernmost parts of the northwestern shelf (further north than 81°N) were ice covered with lower SIC, and by September the northwestern shelf was completely ice-free. Earlier in winter (January and February), open water was observed between 81 and 82°N, off the continental slope north of Spitsbergen. During the March cruise, the northernmost stations off the continental slope were covered by sea ice but located only 10 km from open water. By May, stronger southward ice drift had brought in sea ice to cover the area north of the slope (Fig. 2c and d). The winds remained northerly in the northernmost parts of the Barents Sea in June and July (not shown). This pushed sea ice into the Barents Sea shelf from the north throughout these early summer weeks (Fig. 2), and even though the sea ice melted in the southern parts of the focus area, sea ice still occupied our focus area on the shelf north of 80°N until the end of July (Fig. 1c). In August and September, the northwestern Barents Sea shelf was ice-free, and the ice edge had receded far north off the continental slope.

3.2. Hydrography

Throughout the year, the regions south of the Polar Front (~77°N) and north of the continental shelf break (~81°N) are characterized by relatively warm and saline Atlantic Water from the surface all the way to the bottom. In our focus region, north of the Polar Front and south of the Atlantic Water Boundary Current at the continental slope, the water column is more intricately layered, with a distinct sea ice-influenced surface layer (Fig. 3). The hydrographic changes during the different seasons coincided with the seasonal patterns of both the atmosphere and sea ice (Fig. 1). In March and May, a cold (<−1.5 °C) and relatively fresh (~34.5 g kg^{-1}) winter mixed layer occupied the upper ~ 75–100 m on the northwestern shelf (77–81°N). We call this layer the "Polar Water layer" following the water mass definitions of Sundfjord et al. (2020). Remnants of this layer were still evident in July, but it was then overlaid by a shallow meltwater-stratified surface layer (~8 m thick), which we

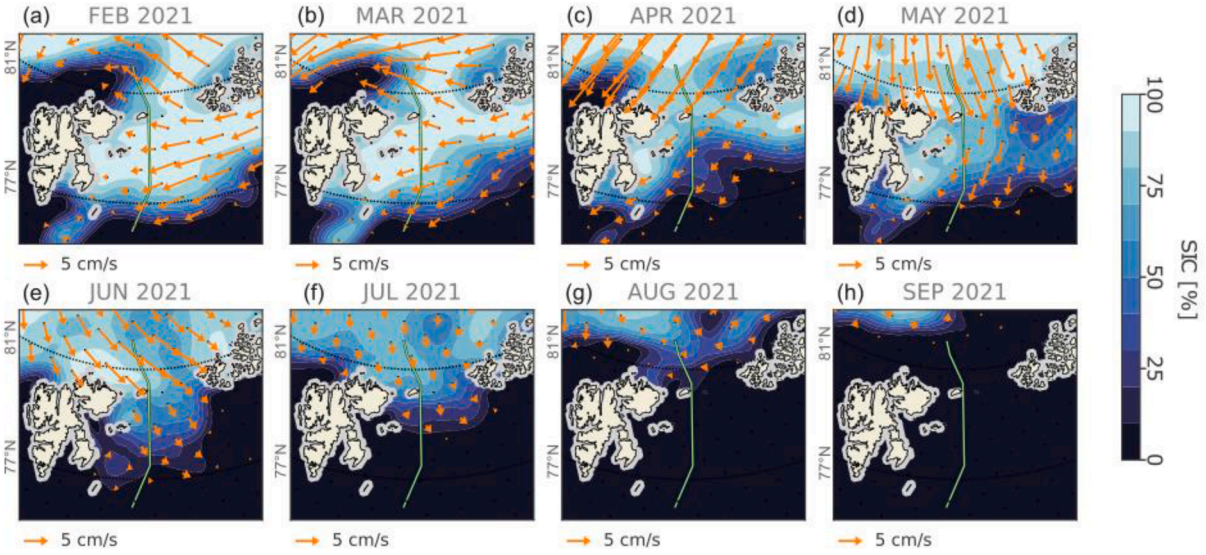

Fig. 2. Monthly mean sea ice concentration and sea ice drift in the northern Barents Sea region. Shading shows sea ice concentration (SIC). Orange arrows indicate sea ice drift. Mean sea ice drift was computed with days with no drift included as zero and subsampled every 100 km. The green line indicates the full transect.

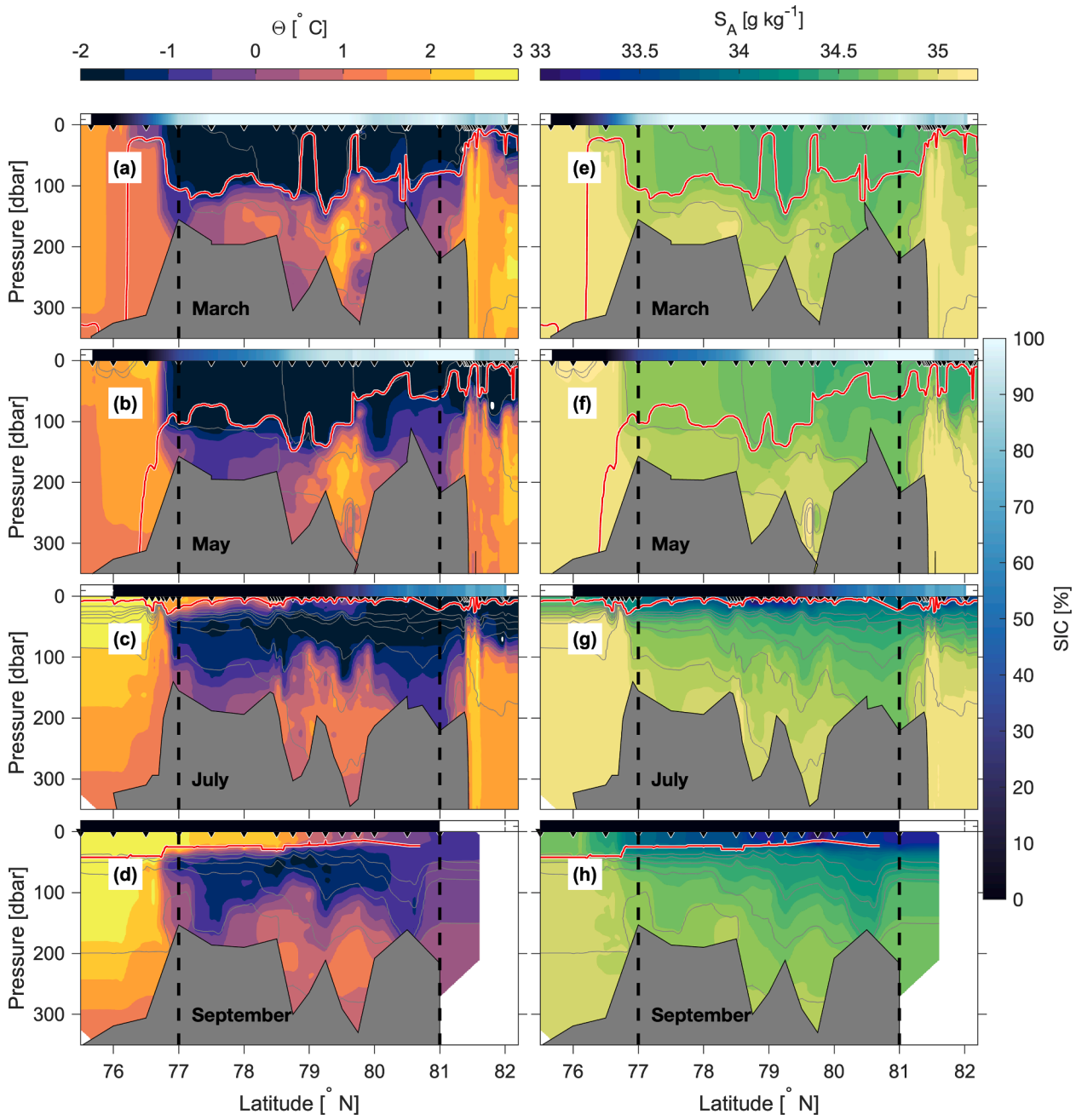

Fig. 3. Sections of Conservative Temperature (left panels) and Absolute Salinity (right panels) in March (a, e), May (b, f), July (c, g) and September (d, h). The focus area on the northwestern Barents Sea shelf from 77 to 81 °N is between the vertical dashed black lines. Locations of CTD stations are indicated with black triangles on top. Isopycnals are indicated with grey isolines. The mixed layer depth is shown with a red line. Sea ice concentration (SIC) is extracted at each station of the transect and indicated in the bar on top of the temperature and salinity panels. The sections are obtained using a Laplacian spline interpolation method with tension, choosing a 60 km search radius and no smoothing (Smith and Wessel, 1990; Pickart and Smethie, 1998).

refer to as the summer surface layer, corresponding to the "Warm Polar Water" definition of Sundfjord et al. (2020). In July, the surface layer was fresher due to sea ice melt ($S_A \sim 33.5$ g kg^{-1}) and warmer (0–1.5 °C) due to increased solar heating. At the end of summer, in September, the summer surface layer had warmed (>2 °C), freshened (<33.5 g kg^{-1}), and deepened to approximately 20–30 m (Fig. 3d, h). The deepening was strongest in the southern half of our focus region. The surface warming reached further north in September than in July, corresponding to the area north of 80°N being ice-free since early July (Fig. 1). South of the Polar Front we observe a seasonal warming of the surface layers, which penetrates downward in the water column throughout the season (Fig. 3).

To further visualise the seasonal evolution, average vertical profiles from our focus region (77–81°N) for each cruise are shown in Fig. 4. They confirm a cold and deep, homogeneous winter mixed layer (Polar Water) from the surface to ~ 75 m in March and ~ 100 m in May, that gradually increased in salinity from March to May (Fig. 4b). It thus appears that the convective winter season, which involves sea ice growth and brine release, persisted until after the March expedition but may have ceased before the May expedition. By July, a surface layer characteristic of summer had formed, exhibiting significantly lower salinity from the surface down to a depth of 50 m. Surface temperatures in July were higher than in March and May, as shown in Fig. 4a-b. From May to July there was also an increase in temperature within the deeper

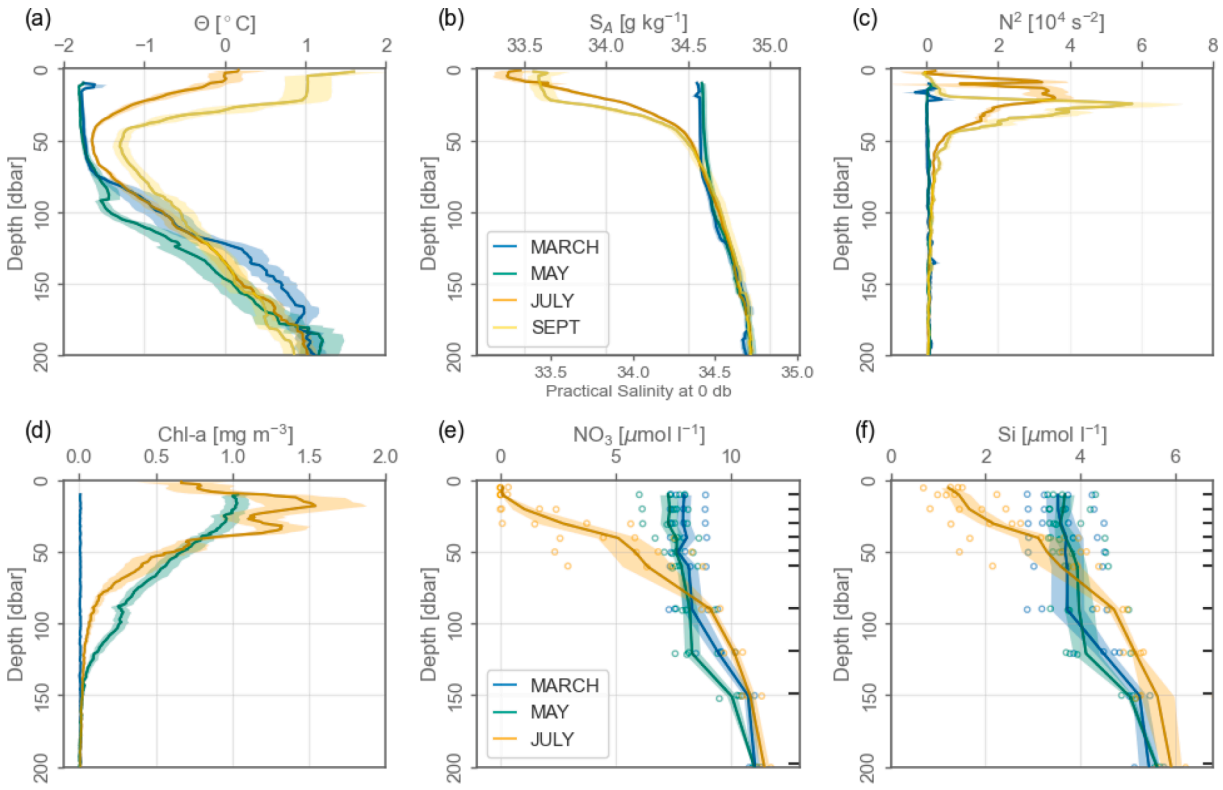

Fig. 4. Vertical profiles of averaged a) Conservative Temperature, b) Salinity (Absolute Salinity S_A on the top x-axis and Practical Salinity on the lower x-axis), c) buoyancy frequency squared N^2 (after vertical smoothing with a 5 dbar running mean), and d) calibrated chlorophyll-*a* fluorescence from the northwestern Barents Sea shelf (77 to 81°N along the transect) of the CTD stations (thick curves) and the standard error of the mean (in shading), from the expeditions in March (blue), May (green), July (orange) and September (yellow). Mean profiles include one CTD profile per station. Vertical profiles of e) nitrate and f) silicic acid from discrete samples (coloured dots) collected at Stations P2-P5, with sampling depths shown as black bars to the right. Chlorophyll-*a* and nutrient data are not available for the September cruise.

parts of the water column (50–150 m). This is not attributed to solar heating but is more likely a result of lateral advection (e.g. from the northern slope of Svalbard or an eddy). Towards the end of summer in September, the temperature of the surface layer had increased by 1 °C from July. Furthermore, the surface layer had undergone deepening, which is evident from the increased mixed layer depth (Fig. 3g, h). This deepening is likely a result of wind energy input into the ocean and entrainment from the Polar Water layer beneath the pycnocline, as illustrated by the comparison of the orange and red curves in Fig. 4b. During the same period, the temperature at approximately 50 m depth, just below the halocline, increased from approximately − 1.5 to − 1.2 °C (Fig. 4a, comparing the orange and red curves), indicative of vertical mixing with the warmer surface layer above and/or the Atlantic layer below, although the salinity did not change at this depth. While the winter water column primarily consisted of two distinct layers, the summer water column had a three-layer structure, with a relatively cold and more saline layer of Polar Water sandwiched between the summer surface and Atlantic Water layers (also evident from Fig. 5). In March and May, the stratification index (N^2) was close to zero, meaning a very weakly stratified water column and small density gradients. In contrast, in July, as the surface layer developed, the stratification increased down to a depth of approximately 50 m, leading to the largest density gradient at 20 m depth in July and 35 m depth in September.

Examining the hydrographic data in temperature-salinity space (Fig. 5), confirms that during winter and spring in the northwestern Barents Sea shelf, two primary water masses prevailed: a winter mixed layer consisting of Polar Water (core temperature −1.7 °C and salinity 34.6 g kg^{-1}) and denser water that results from mixing between Atlantic Water and Polar Water (core temperature around 1 °C and salinity 34.8 g kg^{-1}). Fig. 5 further shows that the two water masses were mixing along a line between the two cores. The summer surface layer, which constitutes the third water mass, was found in July and September, and extends throughout the entire transect in September.

3.3. *Dissolved inorganic nutrients*

Mean vertical profiles of nitrate and silicic acid in the focus area showed relatively low variability and were quite homogeneous in the upper 80 and 120 m in March and May, respectively (Fig. 4 e, f) following the evolution of the winter mixed layer. Looking at individual profiles in March there was a gradual increase in both nitrate and silicic acid concentrations in the upper 90 m from south (P2) to north (P5) (Fig. 5 and S2). Below the surface mixed layer, concentrations of both nitrate and silicic acid increased towards the deeper Atlantic Water. The difference in average surface (upper 90 m) nitrate and silicic acid concentrations in March between Atlantic station P1 and the focus area ranged from 3.4 μmol L^{-1} at station P2 to 2 μmol L^{-1} at station P5 for nitrate and 1.9 μmol L^{-1} (P2) to 0.5 (P5) μmol L^{-1} for silicic acid (Fig S2). In May, the beginning of nitrate surface depletion was detectable in the upper 40 m, and by July, nitrate concentrations were below the detection limit in the upper 10 to 20 m, corresponding to the surface layer (Fig. 4e). Silicic acid concentrations followed a similar pattern but residual concentrations of about 1 μmolL^{-1} remained in the surface waters in July (Fig. 4f). This was also reflected in a seasonal shift in the average nitrate to silicic acid molar ratio for the upper 90 m for the focus area from about 2.3 in March to 1.4 in July (not shown). In July, the shoaling of the nutricline from south to north along the transect was clearly visible for nitrate, phosphate, and silicic acid (Fig. S2) and corresponded well with the depth of the chlorophyll-*a* maximum (Fig. 6c). In July, nitrite showed a different vertical pattern than the other macronutrients

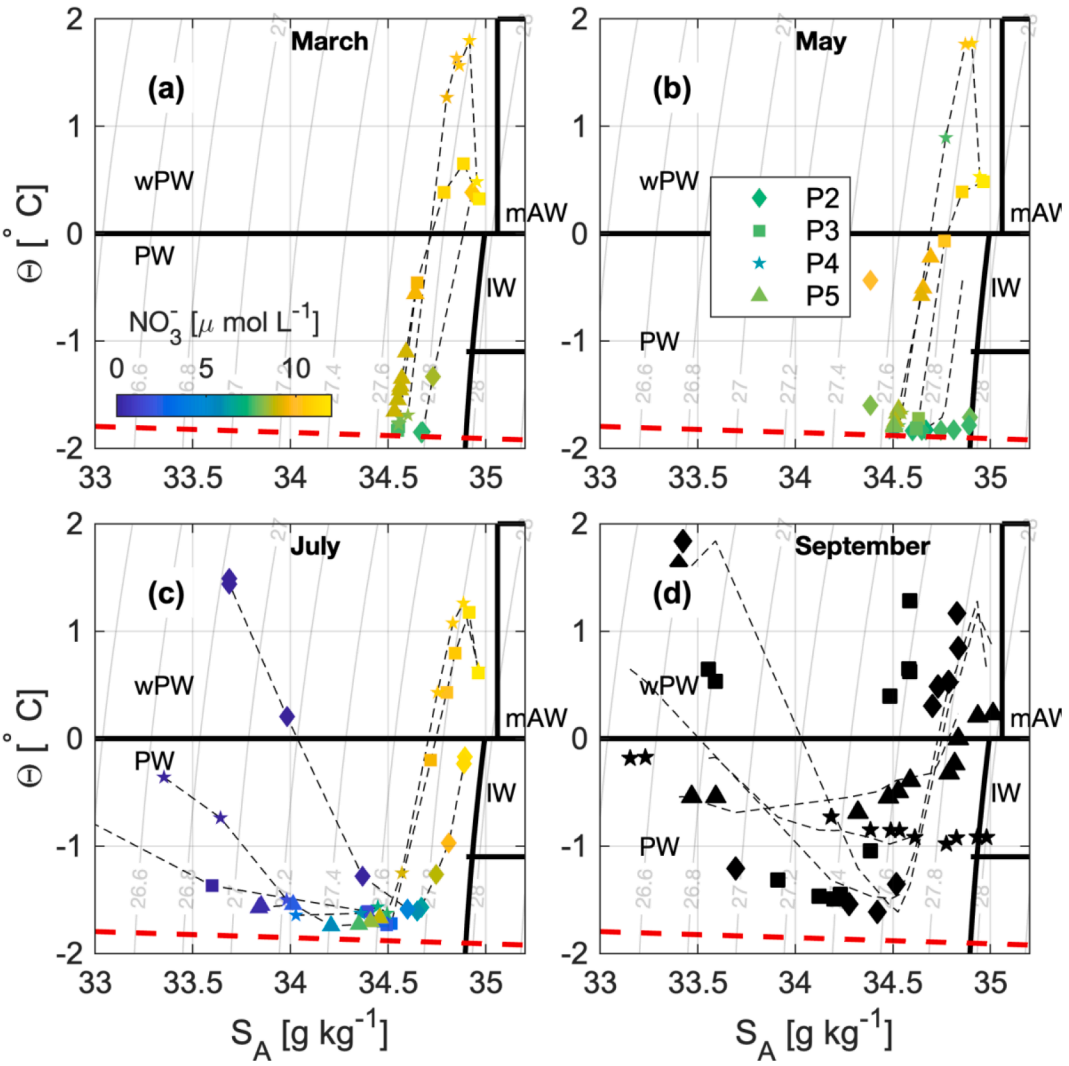

Fig. 5. Temperature-Salinity diagrams at the P-stations color coded with the nitrate concentrations for a) March, b) May, and c) July. d) Temperature-Salinity diagram at the P-stations in September (for consistency symbols shown at the same standard depths that nutrient data was from in the previous months). Lines of equal density are depicted as thin grey curves. The water masses are based on Sundfjord et al. (2020). wPW: warm Polar Water; PW: Polar Water; mAW: modified Atlantic Water; IW: Intermediate Water. The black dashed lines are the T-S profiles where the water samples (with a marking) were from. The red dashed lines indicate the freezing temperature.

with elevated concentrations aligned with the bottom of the mixed layer and a decline both above and below it (Fig. S2).

3.4. Phytoplankton biomass

In March, chlorophyll-*a* concentrations of < 0.1 μg L^{-1} indicate very low phytoplankton biomass (Fig. 6a). Measured particulate organic carbon (POC) concentrations were also low and mostly below 30 μg L^{-1} (Sandven et al., 2023). By May, chlorophyll-*a* concentrations had increased to 1 μg L^{-1} in the upper ~ 50 m of the water column in waters covered by 50 to nearly 100 % of sea ice (Fig. 6b). It is noteworthy that the surface stratification was still very weak in May and the mixed layer depth extended deep, as sea ice melt had not yet started. The Atlantic Water-influenced open water station P1 had elevated (~1 μg L^{-1}) and relatively homogenous chlorophyll-*a* concentrations down to 200 m depth possibly as a result of a storm-induced mixing event during the time of sampling (Ludvigsen et al., 2022). Beam attenuation followed a near-identical pattern as chlorophyll-*a* (Fig. 6e). In July, there was a distinct subsurface chlorophyll-*a* maximum along and just below the pycnocline. This maximum shoaled towards the bottom of the mixed layer at the sea ice edge from 80°N and northwards (Fig. 6c). Here, beam attenuation measurements followed a similar but not identical pattern, with higher values closer to the surface (0–25 m depth). During all seasons elevated beam attenuation values were detected in the bottom boundary layer (Fig. 6d-f). This feature was not visible in chlorophyll-*a* concentrations (Fig. 6a-c).

3.5. Light environment

In March, the measured PAR was below the estimated compensation irradiance throughout the water column, following the calculations described in section 2.1.1c. At 50 m, the PAR values were well below 1 μmol photons m^{-2} s^{-1} in the study area (Fig. 7a). Furthermore, given that the mixed layer depth was generally > 100 m in March (Fig. 3a), the average light levels in the mixed layer were not sufficient to sustain phytoplankton biomass build-up. By May (Fig. 7b), the increase in day length (24 h daylight) and mean solar zenith angle led to isolume depths extending down to 40 m, frequently above a compensation irradiance of 4 μmol photons m^{-2} s^{-1} close to the surface. However, the isolume depths did still not extend beyond the mixed layer depth, as shown in Fig. 3. There is a large variability between different stations, and moreover between isolume depths for the varying compensation

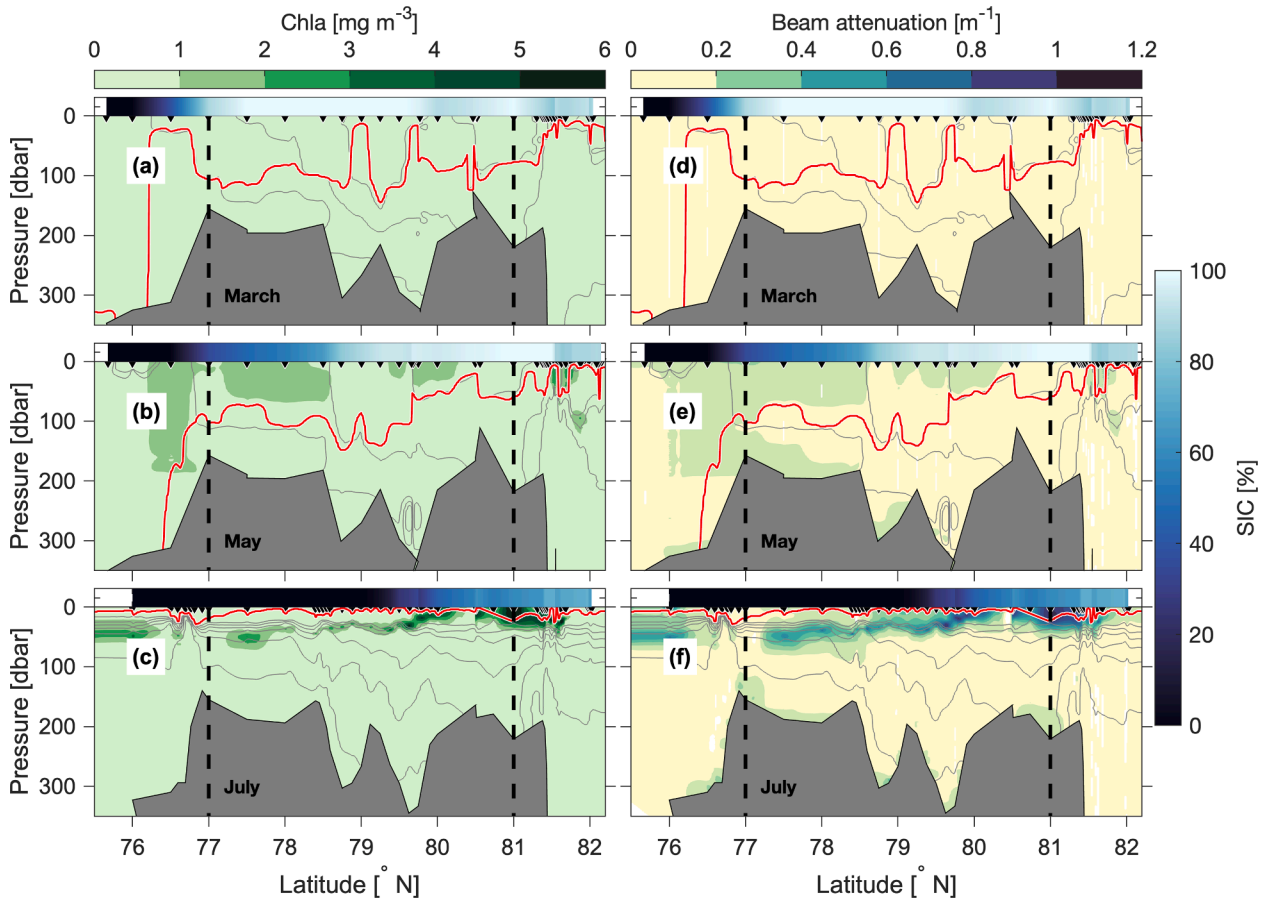

Fig. 6. Sections of chlorophyll-*a* (Chla, left panels) from fluorescence corrected with sampled chlorophyll-*a* and beam attenuation (right panels) in March (a,d), May (b, e) and July (c, f). The focus area from 77 to 81°N is outlined with vertical black dashed lines. Location of CTD stations is indicated with black triangles on top. Isopycnals are indicated with grey curves. The mixed layer is the red line. Sea ice concentration along each transect is indicated on top of the panels.

irradiance estimates. Uncertainties connected to the extrapolation of the measurements could also be significant for near-surface values.

In July, the estimated isolume depths follow a more distinct meridional structure, with the largest depths in open water near the Polar Front extending to 60 m, and near-zero isolume depths under the ice north of 79°N (note the large uncertainties in these estimates). Between 77°N and 79°N the chlorophyll-*a* subsurface maximum seems to follow the isolume depth estimates (Fig. 6c and 7c). The high PAR values measured at depth, between approximately 76.5°N and 77.5N and north of 81.5N, were associated with areas of low surface chlorophyll-*a* concentrations. Self-shading by the surface or subsurface chlorophyll-*a* maximum can explain the lower PAR values for the northern part of the study area, and the corresponding isolume depths were estimated to be close to 0 m. The self-shading is supported by the linear relationship between the diffuse attenuation coefficient K_D and chlorophyll-*a* concentration ($R^2 = 0.63$), found for measurements between 41 and 60 m (Fig S1). However, self-shading did likely not play a major role in limiting phytoplankton growth in the study area since the chlorophyll-*a* maximum was generally situated above 50 m. Variations in light availability at 50 m depth during May and July can also partly be attributed to the diurnal sun cycle (illustrated by the marker color in Fig. 7) and changing cloud cover. SIC seemed to have less influence on the underwater light levels than expected, but the local SIC at the exact time and location of the cast could differ strongly from the larger-scale satellite estimates. Some bias may be introduced from conducting the CTD casts in leads of open water, which is often preferred for practical reasons.

3.6. Heat, freshwater, and chlorophyll-a content

The ocean heat content in the upper 100 m was low north of the Polar Front (77°N) in March and May and increased in July from the front to 80°N, where the sea ice edge was at the time (Fig. 8a; see also Fig. 2a). In September heat content had increased along the entire transect, also north of 80°N, where the sea ice had melted and retreated in August. The freshwater content of the upper 100 m was higher in our focus area than either south or north of the area (Fig. 8b), also in winter and spring. This difference is likely attributed to the substantial import of sea ice (Fig. 2), which subsequently melts within our focus area. The freshwater content decreased from March to May due to sea ice formation and brine release. It increases by ~ 1.2 m from May to September to a total of 2.5–3 m between 77 and 81°N with sea ice melt and the development of the surface mixed layer in summer (Fig. 9b). In the part of the focus area that was ice-free in July, from 77 to 80°N, the freshwater content did not increase from July to September, however, it increased in the northernmost part north of 80°N.

Integrated chlorophyll-*a* standing stocks for the upper 100 m were ~ 0 mg m^{-2} along the entire transect in March and increased significantly by May to ~ 100 mg m^{-2} north of the Polar Front while it declined towards the northern end of the focus area with more sea ice (Fig. 8c). One notable exception was a bloom of > 300 mg m^{-2} at ~ 80.5°N (Fig. 8c). In July, chlorophyll-*a* standing stocks were generally lower than in May except in ice-covered waters north of ~ 80°N (Fig. 8c). Maximum chlorophyll-*a* standing stocks of ~ 150 mg m^{-2} south of the Polar Front and > 250 mg m^{-2} at the shelf slope were associated with Atlantic Water also reflected in the higher heat and lower freshwater content (Fig. 8a-c).

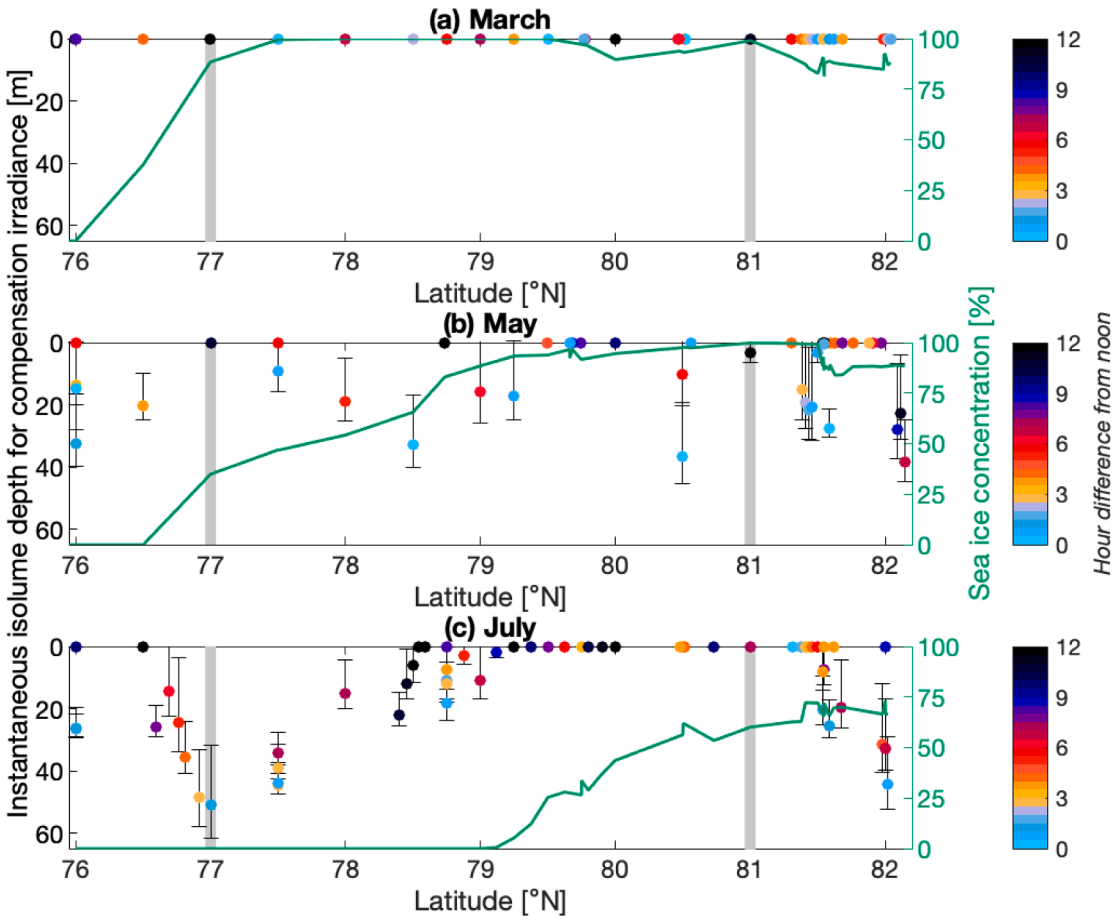

Fig. 7. Isolume depths for the compensation irradiance (here assumed to be 10 μmol photons m^{-2} s^{-1}), estimated from PAR measurements from the CTD casts along the transect. a) In March. b) In May and c) in July. Marker colour indicates the time of day the cast was made; light blue is close to local noon (approximate time for maximum incident solar radiation), and black is close to local midnight. Error bars show isolume depths for other estimates of the compensation irradiance (4 and 15 μmol photons m^{-2} s^{-1}). The grey vertical lines indicate the southern and northern limits of the focus area, green lines show sea ice concentrations.

We investigated if the intensity of the warming of the upper ocean is driven by the duration of ice-free time prior to our measurements. We compared the development of heat content of the upper ocean and the surface mixed layer temperature and depth with the number of days with open water prior to a CTD station being occupied (Fig. 9). The number of days with open water was largest furthest south on the transect and decreased towards the north, as expected given that the ice edge melts and retreats northwards through the summer (Fig. 9a, compare with Fig. 1c). The heat content of the upper 100 m increases with the number of ice free days (Fig. 9b), and when considering only the area within the northwestern Barents Sea (77–81°N), the correspondence between heat content and days with open water is significant (Fig. 9b). Similarly, the surface mixed layer depth increases with time (Fig. 9c), and though its temperature increases from surface heat fluxes with the number of days with open water through the summer, the temperature levels may level off due to the deepening of the surface mixed layer and entrainment from the colder Polar Water layer below.

4. Discussion

4.1. Influence of ice-ocean coupling on upper ocean stratification

Between March and September of 2021, we observed the seasonal transformation of the northwestern Barents Sea shelf system as it shifted from a weakly stratified, ice-covered ocean to a more strongly stratified ice-free ocean. This change is in line with the typical seasonal pattern observed in Arctic shelf seas, where the winter months are characterised by ice cover and the summer months by sea ice retreat (Onarheim et al., 2018). Although the Barents Sea experiences significant year-to-year variations in its sea ice conditions (Efstathiou et al., 2022), the 2021 observations align with this seasonal pattern. In this study, we found that the timing of sea ice melt (and/or retreat) largely determines the warming of the upper ocean, because surface warming (by solar heating) accelerates when the ice has disappeared. In March and May, sea ice thicknesses of about 0.5 to 1 m were observed at the P stations (Ludvigsen, 2022), which is similar to thicknesses observed by King et al. (2017) for locally formed ice in the same area in 2014, while imported ice tends to be thicker (King et al., 2017). We found that the freshwater content increased by 1.0–1.5 m from May (pre-melt) until September, suggesting that there likely was an additional freshwater source other than locally formed sea ice in the northwestern Barents Sea in 2021. Other sources of freshwater include sea ice import, precipitation, and glacial runoff; however, the runoff seems to be largely constrained to near-coastal waters (cf. Petit et al., 2022), and precipitation is small compared to sea ice melt (not shown). Ice drift patterns in 2021 indeed suggest an influx of sea ice from the north in the summer (Fig. 2), while the ice was melting in the south.

In winter 2018/2019 there was a substantial import of thicker sea ice to the Barents Sea, which added significant amounts of freshwater to the upper ocean in the northern Barents Sea and re-stratified and re-cooled the ocean to conditions prior to the extremely warm and saline year 2018 (Aaboe et al., 2021). Both ocean heat and freshwater content returned to pre-2010 levels due to this large sea ice import event in 2019. Our observations in late 2021 have similar freshwater content

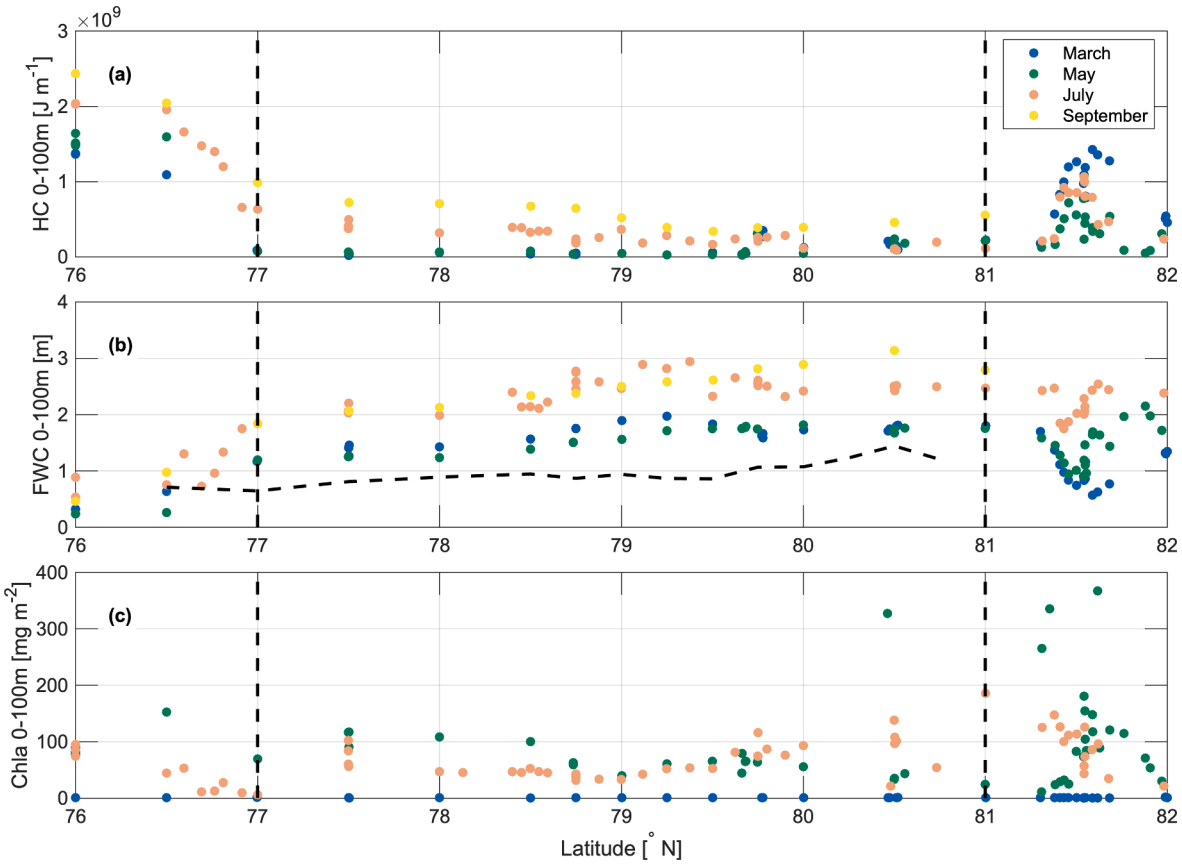

Fig. 8. Development of a) ocean heat, b) freshwater content, and c) integrated chlorophyll-*a* (Chla) over the upper 100 m from March to September. The dashed line in panel b) is the freshwater content increase from May to September. March: blue dots, May: green dots, July: orange dots, and September: yellow dots. Note no chlorophyll-*a* measurements exist for September.

(around 2–3 m) to those observed pre-2010s (Aaboe et al., 2021), which suggests that conditions at the end of 2021 were representative of an Arctic-like ocean climate. Less sea ice import into the northwestern Barents Sea in the future would likely reduce sea ice meltwater-induced stratification (Lind et al., 2018). The freshwater-induced stratification is counterbalanced by the wind energy input into the ocean that tends to increase with less sea ice cover (e.g. Meyer et al., 2017), and we see this as a deepening of the surface mixed layer over summer that is related to the number of ice-free days. Stratification is one of the key factors controlling the initiation of the phytoplankton bloom by restricting the vertical extent of mixing. However, as our results show, it is not the only driver since we observed the initiation of a phytoplankton bloom in a deep winter mixed layer (Fig. 6b).

4.2. Controls on light climate

Another key driver for primary production, especially at the start of the growth season, is light availability in the surface mixed layer (Randelhoff et al., 2019). The light climate in ice-covered waters such as in the Barents Sea is controlled by the solar zenith angle, which gives strong seasonality of the incoming sunlight, cloud cover, and sea ice including small-scale features like snow and melt ponds (Bélanger et al., 2013; Leu et al., 2015; Lebrun et al., 2023). Both sea ice and clouds drastically reduce the available light in the water column. However, the properties of in-water constituents also affect the light climate (Connan-McGinty et al., 2022). While surface heating is largely related to the absence of sea ice (number of ice-free days (SIC < 15 %) with effective solar heating), the variation in light absorption and attenuation in the northern Barents Sea water column is largely dominated by particulate matter (Sandven et al., 2023). The observations support the fact that absorption by CDOM (colored dissolved organic matter) is low and rather stable in such Atlantic-dominated waters (cf. Hancke et al., 2014; Makarewicz et al., 2018; Petit et al., 2022; Sandven et al., 2023), nevertheless in the absence of particulate matter (i.e. before vernal blooms), CDOM still dominates (Sandven et al., 2023).

In the surface layer, phytoplankton biomass governs the light climate variability as evidenced by the close connection of diffuse attenuation coefficient of PAR and chlorophyll-*a* concentration (see supplementary Fig. S1), and the increase of beam attenuation goes hand in hand with phytoplankton biomass build-up (Fig. 6), except near the bottom, where there is resuspension of bottom sediments. Beam attenuation, often used as a POC concentration proxy (see e.g. Sandven et al., 2023), follows to a great extent the chlorophyll-*a* patterns (Fig. 6), which indicates that phytoplankton growth drives the observed increase in POC in surface waters in spring. The partial decoupling of beam attenuation and chlorophyll-*a* in surface waters in July, see also Supplementary Fig. S3, suggests a stronger contribution of non-chlorophyll-*a* containing particles such as detrital material emanating from remnants of an earlier surface bloom and/or heterotrophic organisms sustained by the bloom. This is supported by a seasonal shift from an autotrophic towards a more heterotrophic pelagic community (Kohlbach et al., 2023) and a larger detrital component in the vertical export flux during the summer (Bodur et al., 2023). Bio-optical proxies of chlorophyll-*a* (*in situ* fluorescence) and POC (beam attenuation at 650 nm) also showed some distinct patterns seasonally and spatially (Sandven et al., 2023). There were typically much lower chlorophyll-*a* to phaeophytin ratios in July (Fig. S4) indicative of more grazing or senescent algae by summer.

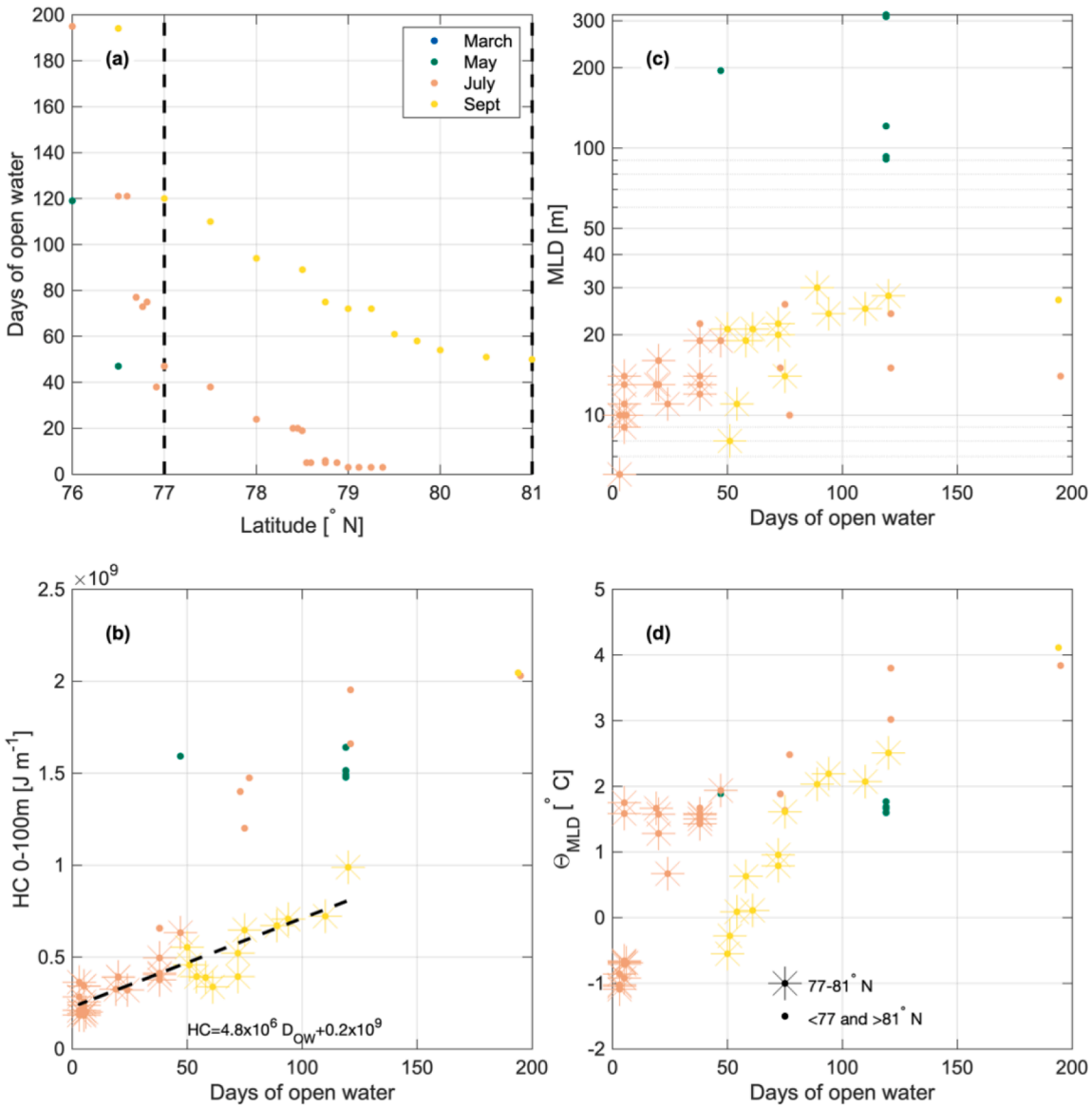

Fig. 9. a) number of days of open water prior to each CTD station, shown with latitude (if no days with open water, no data were shown for the 4 cruises); b) heat content development of the upper 100 m shown with days of open water across the entire section. The stars are for our focus area (77–81°N) with the best-fit indicated (dashed line). D_{OW}: days of open water. c) Development of the surface mixed layer depth (MLD) with D_{OW}. d) Development of the temperature of the surface mixed layer (MLD) with days of open water. The four cruises are colour-coded: March in blue, May in green, July in orange, and September in yellow. In all panels, the stars are for our focus area (77–81°N).

4.3. Seasonal progression of phytoplankton growth limitation

In addition to light and stratification, the availability of nutrients (particularly nitrate in this region) is also a key constraint of phytoplankton growth. Light controls the timing of phytoplankton production while nutrients set an upper limit to phytoplankton biomass build-up (Assmy et al., 2019). The seasonal transition from light limitation in spring towards nutrient limitation in late summer in Arctic waters is strongly influenced by the seasonal evolution of sea ice and sea ice melt-induced upper ocean stratification (Ardyna et al., 2020).

At the end of winter in March, surface nutrient concentrations were at their annual maximum as a result of autumn and winter mixing, replenishing surface nutrient concentrations (Koenig et al., 2023; Jones et al., 2023). The higher late winter nutrient concentrations in Atlantic waters south of the Polar Front (P1) and at the northern shelf slope (P6) compared to our focus area can be explained by differences in stratification regimes. The thermocline in Atlantic waters is generally weaker than the halocline in Arctic waters (Wassmann et al., 2006; Lundesgaard et al., 2022). Furthermore, at P1, phytoplankton was observed down to 200 m depth. Such observations of deep phytoplankton were also made in a similar Atlantic regime south of the Polar Front in the spring of 1998 (Reigstad et al., 2002). The phytoplankton was found at depth due to wind-induced mixing, as suggested by numerical modeling of wind effects on ecosystems in the Barents Sea (Le Fouest et al., 2011).

The higher late winter nutrient concentrations in the northern compared to the southern part of our focus area, despite the northward increasing freshwater content, suggests that the presence of warmer water of Atlantic origin at depth in the northern part of the Barents Sea (see Fig. 3) supplies more nutrients to the surface. These differences in nutrient inventories at the end of winter in the upper 100 m of our focus area indicate differences in winter "mixing efficiency" between more and less Atlantic-influenced locations as AW is the main source of nutrients to the region (Duarte et al., 2021). At that time of the year, phytoplankton uptake had a negligible impact on nutrient profiles since

phytoplankton growth was strongly limited by low light levels in a deep mixed layer and compensation irradiance isolume depths very close to the surface which was reflected in the very low chlorophyll-*a* concentrations.

The marked increase in chlorophyll-*a* in May showed that the spring bloom was initiated in ice-covered waters. Melt ponds had not formed by May and hence played no role in the initiation of the spring bloom in contrast to massive phytoplankton blooms below ponded sea ice in the Chukchi Sea during July (Arrigo et al., 2012, 2014). Measured snow thicknesses of 4.5 to 13.5 cm are within the climatological range for the area (Lee et al., 2021) suggesting that light attenuation by snow was likely not unusual in 2021. The bloom initiated in a deep mixed layer comparable or even deeper than the situation in March, suggesting that the seasonal increase in light and opening between ice floes (cf. Assmy et al., 2017) was sufficient to move the compensation irradiance isolume depths shallow enough to allow production to exceed losses and accumulation of phytoplankton biomass to occur. The estimated compensation irradiance isolume depths, approximately between 20 and 40 m, coincide with the beginning of nitrate depletion in the upper 40 m in May, which may suggest that the actively mixing layer was shallower than the mixed layer. This was also reflected in elevated chlorophyll-*a* concentrations largely restricted to the upper 50 m. Our results contrast with the common assumption that surface stratification (in the upper 20–30 m depth) is a prerequisite for phytoplankton spring bloom initiation and indicates that small changes in actively mixing layer depth can have important implications for spring bloom initiation (Brody and Lozier, 2015).

By July, nutrients, particularly nitrate, were depleted in the upper 10–20 m of the water column coinciding with sea ice melt-induced stratification and shoaling of the mixed layer to depths < 20 m. Surface nutrient depletion was primarily due to uptake by phytoplankton, but dilution by sea ice melt might have also played a minor role. Nitrate showed the deepest and strongest depletion of the three major macronutrients confirming that primary productivity at this time of the year is primarily nitrate-limited within the euphotic zone. The chlorophyll-*a* maximum and nitracline were largely below the pycnocline, implying that stratification acted as a barrier for wind-driven vertical mixing and nitrate replenishment at this time of the year. Light limitation played a larger role towards the northern more ice-covered section of the transect, as evidenced by the shoaling of the subsurface chlorophyll-*a* maximum and shallower isolume depth. The July transect can therefore be interpreted as the space-for-time seasonal variability of primary productivity in a water column influenced by melting sea ice.

The vertical gradient in nutrient depletion was most pronounced in nitrate. The nitracline was for the most part below the mixed layer, while the strongest gradients for phosphate and silicic acid were shallower and less prominent. The residual silicic acid relative to nitrate in the surface layer in summer could be due to changes in phytoplankton community composition. Competition between diatoms and non-siliceous phytoplankton, particularly the haptophyte algae *Phaeocystis pouchetii*, for nitrate could account for incomplete utilisation of silicic acid by diatoms and previous studies have suggested summer residual silicic acid concentrations as a sign of *Phaeocystis* dominance (Reigstad et al., 2002, Krause et al., 2018). Diatoms dominated protist standing stocks in May and July (Bodur et al., 2023) with occasional dominance of dinoflagellates and ciliates (unpublished data) while *Phaeocystis* played a minor role. However, we cannot rule out that *Phaeocystis* bloomed in the intervening months as this species usually follows in the seasonal succession after the diatom spring bloom (Assmy et al., 2023, Degerlund and Eilertsen, 2010).

One interesting feature observed in July was the subsurface nitrite peak at top of the thermocline but below the pycnocline (Figure S2). This feature is known as the primary nitrite maximum from lower latitude oceans and commonly found at the bottom of the euphotic zone (Lomas and Lipschultz, 2006). Oxidation of ammonium to nitrite by bacterial nitrification and release by phytoplankton via incomplete assimilatory reduction of nitrate have been identified as the main sources of this excess nitrite (Lomas and Lipschultz, 2006). The fact that the primary nitrite maximum coincided with the nitracline and the bottom of the subsurface chlorophyll-*a* maximum points towards incomplete assimilatory reduction of nitrate supporting the conclusion of release by phytoplankton as the main driver (Lomas and Lipschultz, 2006). However, the primary nitrite maximum likely was a result of complex biological processes, including ammonium oxidation by bacteria and archaea, since elevated bacterial abundances and activity were associated with the subsurface chlorophyll-*a* maximum (Amargant-Arumí et al., 2023).

5. Summary and conclusions

While the long-term changes and interannual variability of the Barents Sea are well documented, the seasonal progression, especially in the seasonally ice-covered part, in the northwest is not well known. Here we used four cruises repeating the same south-to-north transect between March and September 2021 (same seasonal cycle) to observe how sea ice coverage, retreat, and melt influence the hydrography and affect light, nutrient, and phytoplankton dynamics. We found that sea ice meltwater and timing of ice-free conditions in summer shape the environment, controlling heat accumulation, light and nutrient availability, and phytoplankton activity vertically, seasonally, and meridionally.

In March, at the end of winter, the ocean was cold and covered by sea ice, with a homogeneous mixed layer down to 90–120 m depth, replenished nutrient stocks, and very low phytoplankton biomass. In early spring (May), the winter mixed layer had deepened further and was more saline, likely due to continued ice growth between March and May. At this point, the ocean was still largely ice-covered, but chlorophyll-*a* concentrations in the upper 50 m had increased to 1–3 μg L^{-1}, indicating the start of the spring bloom despite the lack of surface stratification. Our data thus suggests that spring bloom initiation in Arctic waters can commence before the classical spring bloom conditions of sea-ice meltwater-induced stratification (Slagstad, 1984, Sakshaug and Skjoldal, 1989, Sakshaug and Slagstad, 1992, Strass and Nothig, 1996, Slagstad and Wassmann, 1996, Wassmann et al., 1999) are met. It also suggests that phytoplankton growth is likely induced at light levels lower than commonly assumed.

In summer sea ice meltwater input forms a low-density, fresher surface layer. This creates stratification and forms a strong pycno- and nutricline that shapes phytoplankton, with subsurface chlorophyll-*a* maxima at the base of the mixed layer following the nutricline in open water. Eventually, nutrients in the surface layer are depleted, limiting further growth there. The number of open water days during summer strongly affects upper ocean heat accumulation, which in turn is important for preconditioning the ocean for next year's sea ice growth. As summer progresses, the fresh surface mixed layer continues to deepen and warm as sea ice continues to retreat. Just below the summer surface layer, the Polar Water layer, remnants of the winter mixed layer, also warms throughout the summer due to vertical mixing with the warmer surface layer above and the Atlantic layer below. By contrast, the Atlantic layer found at depth cools as spring and summer progress. In the northwestern part, where sea ice was still in the melting stage in July, the surface layer was very shallow or absent, and chlorophyll-*a* maxima were found at or near the surface. In general, the summer data in the south-north direction showed a space-for-time seasonal variability in the key physical and biological variables, with the summer situation progressing northwards along the latitudinal transect along with sea ice retreat.

Our results indicate that less freshwater input to a future ice-free Barents Sea will have a positive impact on surface nutrient inventories and will likely result in increased annual new (nitrate-based) pelagic production (at the expense of ice-associated production) and harvestable marine resources from zooplankton to fish. This is consistent with previous studies that have shown a negative impact of sea ice-derived

meltwater stratification on the biological carbon pump (von Appen et al., 2021). Further investigation of the freshwater input to the water column and the strength of the upper ocean stratification is needed.

In the context of climate change, understanding the seasonal dynamics and changes in the Barents Sea, one of the entry points of Atlantic Water into the Arctic, is important. The data were collected in 2021, when the Arctic Dipole was positively contributing to slowing the sea-ice loss (Polyakov et al., 2023). A transition to the negative phase of the Artic Dipole may accelerate the Arctic sea-ice decline and modulate the ocean dynamics of the Barents Sea and its Atlantification as documented in this manuscript. Hence, monitoring the rapid changes underway in the Barents Sea in terms of sea ice, ocean physics, and ecosystem responses, should stay at the forefront of Arctic oceanography. These four cruises repeating an observation transect from March to September 2021, resolving part of the seasonal cycle in the Barents Sea allowed for a better understanding of the tight coupling between sea ice, ocean, and primary productivity in the northwestern Barents Sea.

Funding

This work was funded by the Research Council of Norway through the project The Nansen Legacy (Grant No. 276730). MM and MAG received funding from the European Union's Horizon 2020 research and innovation programme (Grant agreement No. 101003826) via project CRiceS (Climate Relevant interactions and feedbacks: the key role of sea ice and snow in the polar and global climate system). ZK received funding from the Research Council of Norway for the project 'BREATHE: Bottom sea ice Respiration and nutrient Exchanges Assessed for THE Arctic ' (Grant No. 325405).

Declaration of competing interest

The authors declare that they have no known competing financial interests or personal relationships that could have appeared to influence the work reported in this paper.

Data availability

Data will be made available on request.

Acknowledgments

We thank the captain and the crew of R/V *Kronprins Haakon* for their excellent support at sea during the Nansen Legacy expeditions in 2021. We thank the captain, crew and scientists on board R/V *Hellmer Hanssen* and R/V *Johan Hjort* in September 2021. We also like to thank Karley Campbell for discussions on phytoplankton compensation irradiance. Two anonymous reviewers provided constructive suggestions that helped to improve the manuscript.

Appendix A. Supplementary material

Supplementary data to this article can be found online at https://doi.org/10.1016/j.pocean.2023.103174.

References

Aaboe, S., Lind, S., Hendricks, S., Down, E., Lavergne, T., Ricker, R., 2021. Sea-ice and ocean conditions surprisingly normal in the Svalbard-Barents Sea region after large sea-ice inflows in 2019. In: Copernicus Marine Service Ocean State Report, Issue 5, Journal of Operational Oceanography, 14:sup1, s140–s148; https://doi.org/10.1080/1755876X.2021.1946240.

Amargant-Arumí, M., Müller, O., Bodur, Y.V., Ntinou, I.-V., Vonnahme, T., Assmy, P., Kohlbach, D., Chierici, M., Jones, E., Olsen, L.M., Tsagkaraki, T.M., Reigstad, M., Gradinger, R., 2023. Interannual differences in sea ice regime in the north-western Barents Sea cause major changes in summer pelagic production and export mechanisms. Prog. Oceanography 219. https://doi.org/10.1016/j.pocean.2023.103178.

Arashkevich, E., Wassmann, P., Pasternak, A., Riser, C.W., 2002. Seasonal and spatial changes in biomass, structure, and development progress of the zooplankton community in the Barents Sea. J. Mar. Syst. 38 (1–2), 125–145. https://doi.org/10.1016/S0924-7963(02)00173-2.

Ardyna, M., Mundy, C.J., Mayot, N., Matthes, L.C., Oziel, L., Horvat, C., Leu, E., Assmy, P., Hill, V., Matrai, P.A., Gale, M., Melnikov, I.A., Arrigo, K.R., 2020. Under-ice phytoplankton blooms: Shedding light on the "invisible" part of Arctic primary production. Front. Mar. Sci. 7, 608032 https://doi.org/10.3389/fmars.2020.608032.

Arrigo, K.R., van Dijken, G.L., 2015. Continued increases in Arctic Ocean primary production. Prog. Oceanogr. 136, 60–70. https://doi.org/10.1016/j.pocean.2015.05.002.

Arrigo, K.R., Perovich, D.K., Pickart, R.S., Brown, Z.W., Van Dijken, G.L., Lowry, K.E., Swift, J.H., 2012. Massive phytoplankton blooms under Arctic sea ice. Science 336 (6087), 1408. https://doi.org/10.1126/science.1215065.

Arrigo, K.R., Perovich, D.K., Pickart, R.S., Brown, Z.W., Van Dijken, G.L., Lowry, K.E., Swift, J.H., 2014. Phytoplankton blooms beneath the sea ice in the Chukchi Sea. Deep Sea Res. Part II 105, 1–16. https://doi.org/10.1016/j.dsr2.2014.03.018.

Årthun, M., Eldevik, T., Smedsrud, L.H., Skagseth, Ø., Ingvaldsen, R.B., 2012. Quantifying the influence of Atlantic heat on Barents Sea ice variability and retreat. J. Clim. 25 (13), 4736–4743. https://doi.org/10.1175/JCLI-D-11-00466.1.

Assmy, P., Fernández-Méndez, M., Duarte, P., Meyer, A., Randelhoff, A., Mundy, C.J., Olsen, L.M., Kauko, H.M., Bailey, A., Chierici, M., Cohen, L., Doulgeris, A.P., Ehn, J. K., Fransson, A., Gerland, S., Hop, H., Hudson, S.R., Hughes, N., Itkin, P., Johnsen, G., King, J.A., Koch, B.P., Koenig, Z., Kwasniewski, S., Laney, S.R., Nicolaus, M., Pavlov, A.K., Polashenski, C.M., Provost, C., Rösel, A., Sandbu, M., Spreen, G., Smedsrud, L.H., Sundfjord, A., Taskjelle, T., Tatarek, A., Wiktor, J., Wagner, P.M., Wold, A., Steen, H., Granskog, M.A., 2017. Leads in Arctic pack ice enable early phytoplankton blooms below snow-covered sea ice. Sci. Rep. 7, 40850. https://doi.org/10.1038/srep40850.

Assmy, P., Smetacek, V., Montresor, M., Ferrante, M.I., 2019. Algal blooms. In: Schaechter, M. (Ed.), Encyclopedia of Microbiology, fourth ed. Academic Press, pp. 61–76.

Assmy, P., Kvernvik, A.C., Hop, H., Hoppe, C.J., Chierici, M., David, T.D., Bailey, A., 2023. Plankton dynamics in Kongsfjorden during two years of contrasting environmental conditions. Prog. Oceanogr. https://doi.org/10.1016/j.pocean.2023.102996.

Babin, M., 2020. Climate change tweaks Arctic marine ecosystems. Science 369 (6500), 137–138. https://doi.org/10.1126/science.abd1231.

Barton, B.I., Lenn, Y.D., Lique, C., 2018. Observed Atlantification of the Barents Sea causes the Polar Front to limit the expansion of winter sea ice. J. Phys. Oceanogr. 48 (8), 1849–1866. https://doi.org/10.1175/JPO-D-18-0003.1.

Bélanger, S., Babin, M., Tremblay, J.É., 2013. Increasing cloudiness in Arctic damps the increase in phytoplankton primary production due to sea ice receding. Biogeosciences 10 (6), 4087–4101. https://doi.org/10.5194/bg-10-4087-2013.

Berge, J., Heggland, K., Lønne, O.J., Cottier, F., Hop, H., Gabrielsen, G.W., Misund, O.A., 2015. First records of Atlantic mackerel (*Scomber scombrus*) from the Svalbard archipelago, Norway, with possible explanations for the extensions of its distribution. Arctic 54–61. https://doi.org/10.14430/arctic4455.

Bodur, Y.V., Renaud, P.E., Goraguer, L., Amargant-Arumí, M., Assmy, P., Dąbrowska, A. M., Marquardt, M., Renner, A.H.H., Tatarek, A., Reigstad, M., 2023. Seasonal patterns of vertical flux in the northern Barents Sea under Atlantic Water influence and sea-ice decline. Prog. Oceanography. https://doi.org/10.1016/j.pocean.2023.103132.

Brody, S.R., Lozier, M.S., 2015. Characterizing upper-ocean mixing and its effect on the spring phytoplankton bloom with in situ data. ICES J. Mar. Sci. 72 (6), 1961–1970. https://doi.org/10.1093/icesjms/fsv006.

Castro de la Guardia, L., Farinas, T.H., Marchese, C., Amargant Arumı, M., Myers, P.G., Belanger, S., Assmy, P., Gradinger, R., Duarte, P., 2023. Assessing net primary production in the northwestern Barents Sea using in situ, remote sensing and modelling approaches. Prog. Oceanogr. 219, 103160. https://doi.org/10.1016/j.pocean.2023.103160.

Cole, S.T., Timmermans, M.L., Toole, J.M., Krishfield, R.A., Thwaites, F.T., 2014. Ekman veering, internal waves, and turbulence observed under Arctic sea ice. J. Phys. Oceanogr. 44 (5), 1306–1328. https://doi.org/10.1175/JPO-D-12-0191.1.

Dalpadado, P., Arrigo, K.R., van Dijken, Skjoldal, H.R., Bagøien, E., Dolgov, A.V., Sperfeld, E., 2020. Climate effects on temporal and spatial dynamics of phytoplankton and zooplankton in the Barents Sea. Prog. Oceanogr. 185, 102320. https://doi.org/10.1016/j.pocean.2020.102320.

Connan-McGinty, S., Banas, N.S., Berge, J., Cottier, F., Grant, S., Johnsen, G., Kopec, T. P., Porter, M., McKee, D., 2022. Midnight sun to Polar Night: A model of seasonal light in the Barents Sea. J. Adv. Model. Earth Syst. 14 (10), e2022MS003198 https://doi.org/10.1029/2022MS003198.

Degerlund, M., Eilertsen, H.C., 2010. Main Species Characteristics of Phytoplankton Spring Blooms in NE Atlantic and Arctic Waters (68–80° N). Estuar. Coasts 33 (2), 242–269.

Duarte, P., Meyer, M., Moreau, S., 2021. Nutrients in water masses in the Atlantic sector of the Arctic Ocean: temporal trends, mixing and links with primary production. J. Geophys. Res.: Oceans 126, e2021JC017413. https://doi.org/10.1029/2021JC017413.

Efstathiou, E., Eldevik, T., Årthun, M., Lind, S., 2022. Spatial Patterns, Mechanisms, and Predictability of Barents Sea Ice Change. J. Clim. 35 (10), 2961–2973. https://doi.org/10.1175/JCLI-D-21-0044.1.

Ellingsen, I., Slagstad, D., Sundfjord, A., 2009. Modification of water masses in the Barents Sea and its coupling to ice dynamics: a model study. Ocean Dyn. 59, 1095–1108. https://doi.org/10.1007/s10236-009-0230-5.

Eriksen, E., Skjoldal, H.R., Dolgov, A.V., Strand, E., Keulder-Stenevik, F., Prokopchuk, I. P., Benzik, A.N., 2021. Diet and trophic structure of fishes in the Barents Sea: Seasonal and spatial variations. Prog. Oceanogr. 197, 102663 https://doi.org/10.1016/j.pocean.2021.102663.

Fossheim, M., Primicerio, R., Johannesen, E., Ingvaldsen, R.B., Aschan, M.M., Dolgov, A. V., 2015. Recent warming leads to a rapid borealization of fish communities in the Arctic. Nat. Clim. Chang. 5 (7), 673–677. https://doi.org/10.1038/nclimate2647.

Frey, K. E., Comiso, J. C., Cooper, L. W., Grebmeier, J. M., Stock, L. V., 2021. Arctic Ocean Primary Productivity: The Response of Marine Algae to Climate Warming and Sea Ice Decline. NOAA Technical Report OAR ARC ; 21-07. https://doi.org/10.25923/kxhb-dw16.

Gardner, W.D., Richardson, M.J., Mishonov, A.V., Lam, P.J., Xiang, Y., 2022. Distribution, sources, and dynamics of particulate matter along trans-Arctic sections. J. Geophys. Res.: Oceans 127, e2021JC017970. https://doi.org/10.1029/2021JC017970.

Gerland, S., Wold, A., Altuna, N.E., Anglada-Ortiz, G., Arumi, M.A., Bodur, Y., Bratrein, M., Chitkara, C., de Freitas, T.R., Divine, D., Dybdahl, J., Espinel, N., Flo, S., Gawinski, C., Giebichenstein, J., Grytaas, A., Jacobsen, J.A., Jones, E., Jorda, E., Jortveit, A., Karlsson, J., Keck, A., Khuong, D., Kline, S., Kohler, S., Kull, L., Marquardt, M., Müller, O., Nowicki, R., Palmesen, M., Petit, T., Pitusi, V., Sen, A., Steer, A., Steinsland, A., Summers, N., Ziegler, A., 2022 Seasonal cruise Q1 (2021): Cruise report. The Nansen Legacy Report Series, 29/2022. https://doi.org/10.7557/nlrs.646.

Gerland, S., 2022, CTD data from Nansen Legacy Cruise - Seasonal Cruise Q1, NMDC, https://doi.org/10.21335/NMDC-1491279668.

Grasshoff, K., Ehrhardt, M., Kremling, K., 1983. Methods of Seawater Analysis, 2nd revised and extended Edn. Verlag Chemie GmbH, p. 6940.

Gundersen, K., Møgster, J.S., Lien, V.S., Ershova, E., Lunde, L.F., Arnesen, H., Olsen, A.K., 2022. Thirty Years of Nutrient Biogeochemistry in the Barents Sea and the Adjoining Arctic Ocean, 1990–2019. Sci. Data 9 (1), 649. https://doi.org/10.1038/s41597-022-01781-w.

Hancke, K., Hovland, E.K., Volent, Z., Pettersen, R., Johnsen, G., Moline, M., Sakshaug, E., 2014. Optical properties of CDOM across the Polar Front in the Barents Sea: Origin, distribution and significance. J. Mar. Syst. 130, 219–227. https://doi.org/10.1016/j.jmarsys.2012.06.006.

Holm-Hansen, O., Riemann, B., 1978. Chlorophyll a determination: Improvement of the methodology. Oikos 30, 438–447. https://doi.org/10.2307/3543338.

Hordoir, R., Skagseth, Ø., Ingvaldsen, R.B., Sandø, A.B., Löptien, U., Dietze, H., Lind, S., 2022. Changes in Arctic stratification and mixed layer depth cycle: A modeling analysis. J. Geophys. Res. Oceans 127 (1). https://doi.org/10.1029/2021JC017270.

Horvat, C., Bisson, K., Seabrook, S., Cristi, A., Matthes, L.C., 2022. Evidence of phytoplankton blooms under Antarctic sea ice. Front. Mar. Sci. 9, 2154. https://doi.org/10.3389/fmars.2022.942799.

Ingvaldsen, R.B., Asplin, L., Loeng, H., 2004. The seasonal cycle in the Atlantic transport to the Barents Sea during the years 1997–2001. Cont. Shelf Res. 24 (9), 1015–1032. https://doi.org/10.1016/j.csr.2004.02.011.

Ingvaldsen, R.B., Assmann, K.M., Primicerio, R., Fossheim, M., Polyakov, I.V., Dolgov, A. V., 2021. Physical manifestations and ecological implications of Arctic Atlantification. Nat. Rev. Earth Environ. 2 (12), 874–889. https://doi.org/10.1038/s43017-021-00228-x.

Isaksen, K., Nordli, Ø., Ivanov, B., Køltzow, M.A., Aaboe, S., Gjelten, H.M., Karandasheva, T., 2022. Exceptional warming over the Barents area. Sci. Rep. 12 (1), 937. https://doi.org/10.1038/s41598-022-13568-5.

Jakobsson, M., Mayer, L., Coakley, B., Dowdeswell, J.A., Forbes, S., Fridman, B., Hodnesdal, H., Noormets, R., Pedersen, R., Rebesco, M., Schenke, H.W., Zarayskaya, Y., Accettella, D., Armstrong, A., Anderson, R.M., Bienhoff, P., Camerlenghi, A., Church, I., Edwards, M., Gardner, J.V., Hall, J.K., Hell, B., Hestvik, O., Kristoffersen, Y., Marcussen, C., Mohammad, R., Mosher, D., Nghiem, S. V., Pedrosa, M.T., Travaglini, P.G., Weatherall, P., 2012. The International Bathymetric Chart of the Arctic Ocean (IBCAO) Version 3.0. Geophys. Res. Lett. 39 https://doi.org/10.1029/2012gl052219.

Jones, E., Chierici, M., Fransson, A., Assmann, K.M., Renner, A.H.H., Lødemel, H.H., 2023. Inorganic carbon and nutrient dynamics in the marginal ice zone of the Barents Sea: seasonality and implications for ocean acidification. Prog. Oceanogr. 219 https://doi.org/10.1016/j.pocean.2023.103131.

Jones, E., Reigstad, M., Espinel Velasco, N., Gjerland, A., Goraguer, L., Lødemel, H. H., Kline, S., Lind, S., Marsden, L., Maurstad, M., Müller, O., Nordstrand, J.V., Pitusi, V., Stabell, H., & Strombom, E. (2022a). JC2-1 Joint cruise part 1 2021: Cruise report. *The Nansen Legacy Report Series 35/2022*. https://doi.org/10.7557/nlrs.6744.

Jones, E., Chierici, M., Lødemel, H.H., Møgster, J. & Fonnes, L. (2022b). Water column data on dissolved inorganic nutrients (nitrite, nitrate, phosphate and silicic acid) from Process (P) stations during the Nansen LEGACY joint cruise JC2-1, 2021708, with R.V. Kronprins Haakon, 14-24 July 2021, NMDC https://doi.org/10.21335/NMDC-1747434716.

Jones, E., Chierici, M., Lødemel, H.H., Møgster, J. & Fonnes, L. (2022c). Water column data on dissolved inorganic nutrients (nitrite, nitrate, phosphate and silicic acid) from Process (P) stations during the Nansen LEGACY seasonal cruise Q2, 2021704, with R.V. Kronprins Haakon, 30 April - 18 May 2021, NMDC https://doi.org/10.21335/NMDC-487023368.

Jones, E., Chierici, M., Lødemel, H.H., Møgster, J. & Fonnes, L. (2022d). Water column data on dissolved inorganic nutrients (nitrite, nitrate, phosphate and silicic acid) from Process (P) stations during the Nansen LEGACY seasonal cruise Q1, 2021703, with R.V. Kronprins Haakon, 4-17 March 2021, NMDC https://doi.org/10.21335/NMDC-762320451.

Jones, E., 2022. CTD data from Nansen Legacy Cruise -. Joint cruise 2-1, NMDC. https://doi.org/10.21335/NMDC-2085836005.

Kahru, M., Lee, Z., Mitchell, B.G., Nevison, C.D., 2016. Effect of sea ice cover on satellite-detected primary production in the Arctic Ocean. Biol. Lett. 12, 20160223. https://doi.org/10.1098/rsbl.2016.0223.

King, J., Spreen, G., Gerland, S., Haas, C., Hendricks, S., Kaleschke, L., Wang, C., 2017. Sea-ice thickness from field measurements in the northwestern Barents Sea. J. Geophys. Res. Oceans 122, 1497–1512. https://doi.org/10.1002/2016JC012199.

Koenig, Z., Fer, I., Chierici, M., Fransson, A., Jones, E., Kolås, E., 2023. Diffusive and advective cross-frontal fluxes of inorganic nutrients and dissolved inorganic carbon in the Barents Sea in autumn. Prog. Oceanogr. 219 https://doi.org/10.1016/j.pocean.2023.103161.

Koenigk, T., Mikolajewicz, U., Jungclaus, J.H., Kroll, A., 2009. Sea ice in the Barents Sea: seasonal to interannual variability and climate feedbacks in a global coupled model. Clim. Dyn. 32, 1119–1138. https://doi.org/10.1007/s00382-008-0450-2.

Kohlbach, D., Goraguer, L., Bodur, Y.V., Müller, O., Amargant-Arumí, M., Blix, K., Assmy, P., 2023. Earlier sea-ice melt extends the oligotrophic summer period in the Barents Sea with low algal biomass and associated low vertical flux. Prog. Oceanogr. 103018 https://doi.org/10.1016/j.pocean.2023.103018.

Krause, J.W., Duarte, C.M., Marquez, I.A., Assmy, P., Fernández-Méndez, M., Wiedmann, I., Wassmann, P., Kristiansen, S., Agustí, S., 2018. Biogenic silica production and diatom dynamics in the Svalbard region during spring. Biogeosciences 15 (21), 6503–6517. https://doi.org/10.5194/bg-2018-226.

Le Fouest, V., Postlethwaite, C., Maqueda, M.A.M., Belanger, S., Babin, M., 2011. On the role of tides and strong wind events in promoting summer primary production in the Barents Sea. Cont. Shelf Res. 31 (17), 1869–1879. https://doi.org/10.1016/j.csr.2011.08.013.

Lebrun, M., Vancoppenolle, M., Madec, G., Babin, M., Becu, G., Lourenço, A., Delille, B., 2023. Light under Arctic sea ice in observations and Earth System Models. J. Geophys. Res.: Oceans.

Lee, S.-M., Shi, H., Sohn, B.-J., Gasiewski, A.J., Meier, W.N., Dybkjær, G., 2021. Winter snow depth on Arctic sea ice from satellite radiometer measurements (2003–2020): Regional patterns and trends. Geophys. Res. Lett. 48, e2021GL094541 https://doi.org/10.1029/2021GL094541.

Lefort, K.J., Garroway, C.J., Ferguson, S.H., 2020. Killer whale abundance and predicted narwhal consumption in the Canadian Arctic. Glob. Chang. Biol. 26 (8), 4276–4283. https://doi.org/10.1111/gcb.15152.

Nansen Legacy (2022). Sampling protocols: Version 10. The Nansen Legacy Report Series 32/2022. https://doi.org/10.7557/nlrs.6684.

Leu, E., Mundy, C.J., Assmy, P., Campbell, K., Gabrielsen, T.M., Gosselin, M., Gradinger, R., 2015. Arctic spring awakening–Steering principles behind the phenology of vernal ice algal blooms. Prog. Oceanogr. 139, 151–170. https://doi.org/10.1016/j.pocean.2015.07.012.

Lewis, K.M., van Dijken, G.L., Arrigo, K.R., 2020. Changes in phytoplankton concentration now drive increased Arctic Ocean primary production. Science 369, 198–202. https://doi.org/10.1126/science.aay8380.

Lind, S., Ingvaldsen, R.B., 2012. Variability and impacts of Atlantic Water entering the Barents Sea from the north. Deep Sea Res. Part I 62, 70–88. https://doi.org/10.1016/j.dsr.2011.12.007.

Lind, S., Ingvaldsen, R.B., Furevik, T., 2016. Arctic layer salinity controls heat loss from deep Atlantic layer in seasonally ice-covered areas of the Barents Sea. Geophys. Res. Lett. 43 (10), 5233–5242. https://doi.org/10.1002/2016GL068421.

Lind, S., Ingvaldsen, R.B., Furevik, T., 2018. Arctic warming hotspot in the northern Barents Sea linked to declining sea-ice import. NatureClimate Change 8 (7), 634–639. https://doi.org/10.1038/s41558-018-0205-y.

Loeng, H., 1991. Features of the physical oceanographic conditions of the Barents Sea. Polar Res. 10 (1), 5–18. https://doi.org/10.3402/polar.v10i1.6723.

Lomas, M.W., Lipschultz, F., 2006. Forming the primary nitrite maximum: Nitrifiers or phytoplankton? Limnol. Oceanogr. 51 (5), 2453–2467. https://doi.org/10.4319/lo.2006.51.5.2453.

[dataset] Ludvigsen, M. (2022) CTD data from Nansen Legacy Cruise - Seasonal cruise Q2, NMDC, https://doi.org/10.21335/NMDC-515075317.

Ludvigsen, M., Assmy, P., Adams, M.J.S., Arumi, M.A., Bjørkelund, T.M., Bodur, Y., Bremnes, J.E., Flo, S., Gawinski, C., Giebichenstein, J., Halvorsen, E., Hatlebakk, M., Hess, S., Hop, H., Itkin, P., Jones, E., Karlsson, K., Keck, A., Kohlbach, D., Kohler, S. G., Krapp, R., Leopold, P., Marquardt, M., Molina, E.J., Nowicki, R., Olsen, L.M., Ortiz, G.A., Petit, T., Ricardo de Freitas, T., Saubrekka, K., Sen, A., Steer, A., Summers, N., Thiele, S., Thorstensen, H., Vihtakari, M., 2022. Seasonal cruise Q2 2021: Cruise report. The Nansen Legacy Report Series 34/2022 https://doi.org/10.7557/nlrs.6689.

Lundesgaard, Ø., Sundfjord, A., Lind, S., Nilsen, F., Renner, A.H.H., 2022. Import of Atlantic Water and sea ice controls the ocean environment in the northern Barents Sea. Ocean Sci. 18 (5), 1389–1418. https://doi.org/10.5194/os-18-1389-2022.

Makarewicz, A., Kowalczuk, P., Sagan, S., Granskog, M.A., Pavlov, A.K., Zdun, A., Zabłocka, M., 2018. Characteristics of chromophoric and fluorescent dissolved organic matter in the Nordic Seas. Ocean Sci. 14 (3), 543–562. https://doi.org/10.5194/os-14-543-2018.

McDougall, J. & Barker, P., 2011. Getting started with TEOS-10 and the Gibbs Seawater (GSW) Oceanographic Toolbox, 28pp., SCOR/IAPSO WG127, ISBN 978-0-646-55621-5.

Meyer, A., Fer, I., Sundfjord, A., Peterson, A.K., 2017. Mixing rates and vertical heat fluxes north of Svalbard from Arctic winter to spring. J. Geophys. Res. Oceans 122 (6), 4569–4586. https://doi.org/10.1002/2016JC012441.

Muilwijk, M., Nummelin, A., Heuzé, C., Polyakov, I.V., Zanowski, H., Smedsrud, L.H., 2023. Divergence in climate model projections of future Arctic Atlantification. J. Climate 36 (6), 1727–1748. https://doi.org/10.1175/JCLI-D-22-0349.1.

Neukermans, G., Reynolds, R.A., Stramski, D., 2014. Contrasting inherent optical properties and particle characteristics between an under-ice phytoplankton bloom

and open water in the Chukchi Sea. Deep Sea Res. Part II 105, 59–73. https://doi.org/10.1016/j.dsr2.2014.03.014.
Olli, K., Riser, C.W., Wassmann, P., Ratkova, T., Arashkevich, E., Pasternak, A., 2002. Seasonal variation in vertical flux of biogenic matter in the marginal ice zone and the central Barents Sea. J. Mar. Syst. 38 (1–2), 189–204. https://doi.org/10.1016/S0924-7963(02)00177-X.
Omar, A.M., Johannessen, T., Olsen, A., Kaltin, S., Rey, F., 2007. Seasonal and interannual variability of the air–sea CO_2 flux in the Atlantic sector of the Barents Sea. Mar. Chem. 104 (3–4), 203–213. https://doi.org/10.1016/j.marchem.2006.11.002.
Onarheim, I.H., Eldevik, T., Smedsrud, L.H., Stroeve, J.C., 2018. Seasonal and regional manifestation of Arctic sea ice loss. J. Clim. 31 (12), 4917–4932. https://doi.org/10.1175/JCLI-D-17-0427.1.
Oziel, L., Massicotte, P., Randelhoff, A., Ferland, J., Vladoiu, A., Lacour, L., Babin, M., 2019. Environmental factors influencing the seasonal dynamics of spring algal blooms in and beneath sea ice in western Baffin Bay. Elem Sci Anth 7, 34. https://doi.org/10.1525/elementa.372.
Oziel, L., Baudena, A., Ardyna, M., Massicotte, P., Randelhoff, A., Sallée, J.B., Babin, M., 2020. Faster Atlantic currents drive poleward expansion of temperate phytoplankton in the Arctic Ocean. Nat. Commun. 11 (1), 1705. https://doi.org/10.1038/s41467-020-15485-5.
Paulsen, M.L., Dore, H., Garczarek, L., Seuthe, L., Mueller, O., Sandaa, R.A., Larsen, A., 2016. *Synechococcus* in the Atlantic gateway to the Arctic Ocean. Front. Mar. Sci. 3, 191. https://doi.org/10.3389/fmars.2016.00191.
Petit, T., Hamre, B., Sandven, H., Röttgers, R., Kowalczuk, P., Zablocka, M., Granskog, M. A., 2022. Inherent optical properties of dissolved and particulate matter in an Arctic fjord (Storfjorden, Svalbard) in early summer. Ocean Sci. 18 (2), 455–468. https://doi.org/10.5194/os-18-455-2022.
Pfirman, S., Bauch, D., Gammelsrød, T., 1994. The northern Barents Sea: water mass distribution and modification. AGU (American Geophysical Union).
Pickart, R.S., Smethie Jr, W.M., 1998. Temporal evolution of the deep western boundary current where it enters the sub-tropical domain. Deep Sea Res. Part i: Oceanogr. Res. Papers 45, 1053–1083. https://doi.org/10.1016/s0967-0637(97)00084-8.
Polyakov, I.V., Pnyushkov, A.V., Alkire, M.B., Ashik, I.M., Baumann, T.M., Carmack, E. C., Yulin, A., 2017. Greater role for Atlantic inflows on sea-ice loss in the Eurasian Basin of the Arctic Ocean. Science 356 (6335), 285–291. https://doi.org/10.1126/science.aai8204.
Polyakov, I.V., Alkire, M.B., Bluhm, B.A., Brown, K.A., Carmack, E.C., Chierici, M., Wassmann, P., 2020. Borealization of the Arctic Ocean in response to anomalous advection from sub-Arctic seas. Front. Mar. Sci. 7, 491. https://doi.org/10.3389/fmars.2020.00491.
Polyakov, I.V., Ingvaldsen, R.B., Pnyushkov, A.V., Bhatt, U.S., Francis, J.A., Janout, M., Skagseth, Ø., 2023. Fluctuating Atlantic inflows modulate Arctic atlantification. Science 381 (6661), 972–979. https://doi.org/10.1126/science.adh5158.
Randelhoff, A., Fer, I., Sundfjord, A., Tremblay, J.É., Reigstad, M., 2016. Vertical fluxes of nitrate in the seasonal nitracline of the Atlantic sector of the Arctic Ocean. J. Geophys. Res. Oceans 121 (7), 5282–5295. https://doi.org/10.1002/2016JC011779.
Randelhoff, A., Oziel, L., Massicotte, P., Bécu, G., Galí, M., Lacour, L., Dumont, D., Vladoiu, A., Marec, C., Bruyant, F., Houssais, M.N., Tremblay, J., Deslongchamps, G., Babin, M., 2019. The evolution of light and vertical mixing across a phytoplankton ice-edge bloom. Elem. Sci. Anth. 7 https://doi.org/10.1525/elementa.357.
Rat'kova, T.N., Wassmann, P., 2002. Seasonal variation and spatial distribution of phyto- and protozooplankton in the central Barents Sea. J. Mar. Syst. 38 (1–2), 47–75. https://doi.org/10.1016/S0924-7963(02)00169-0.
Reigstad, M., Wassmann, P., Riser, C.W., Øygarden, S., Rey, F., 2002. Variations in hydrography, nutrients and chlorophyll a in the marginal ice-zone and the central Barents Sea. J. Mar. Syst. 38 (1–2), 9–29. https://doi.org/10.1016/S0924-7963(02)00167-7.
Renner, A.H.H., Bailey, A., Reigstad, M., Sundfjord, A., Chierici, M., Jones, E.M., 2023. Hydrography, inorganic nutrients and chlorophyll *a* linked to sea ice cover in the Atlantic Water inflow region north of Svalbard. Prog. Oceanogr. 219 https://doi.org/10.1016/j.pocean.2023.103162.
Renner, A.H.H., Sundfjord, A., Janout, M.A., Ingvaldsen, R.B., Beszczynska-Möller, A., Pickart, R.S., Pérez-Hernández, M.D., 2018. Variability and redistribution of heat in the Atlantic Water boundary current north of Svalbard. J. Geophys. Res. Oceans 123 (9), 6373–6391. https://doi.org/10.1029/2018JC013814.
Riser, C.W., Wassmann, P., Olli, K., Pasternak, A., Arashkevich, E., 2002. Seasonal variation in production, retention and export of zooplankton faecal pellets in the marginal ice zone and central Barents Sea. J. Mar. Syst. 38 (1–2), 175–188. https://doi.org/10.1016/S0924-7963(02)00176-8.
Roesler, C., Uitz, J., Claustre, H., Boss, E., Xing, X., Organelli, E., Barbieux, M., 2017. Recommendations for obtaining unbiased chlorophyll estimates from in situ chlorophyll fluorometers: A global analysis of WET Labs ECO sensors. Limnol. Oceanogr. Methods 15 (6), 572–585. https://doi.org/10.1002/lom3.10185.
Sakshaug, E., Skjoldal, H.R., 1989. Life at the ice edge. Ambio. Stockholm 18 (1), 60–67.
Sakshaug, E., Slagstad, D., 1992. Sea ice and wind: effects on primary productivity in the Barents Sea. Atmos. Ocean 30 (4), 579–591.
Sandø, A.B., Nilsen, J.Ø., Gao, Y., Lohmann, K., 2010. Importance of heat transport and local air-sea heat fluxes for Barents Sea climate variability. J. Geophys. Res. Oceans 115 (C7). https://doi.org/10.1029/2009JC005884.
Sandven, H., Hamre, B., Petit, T., Röttgers, R., Liu, H., Granskog, M.A., 2023. Seasonality and drivers of water column optical properties on the northwestern Barents Sea shelf. Prog. Oceanogr. 217, 103076 https://doi.org/10.1016/j.pocean.2023.103076.
Siegel, D.A., Doney, S.C., Yoder, J.A., 2002. The North Atlantic spring phytoplankton bloom and Sverdrup's critical depth hypothesis. Science 296 (5568), 730–733. https://doi.org/10.1126/science.1069174.
Siwertsson, A., Husson, B., Arneberg, P., Assmann, K., Assmy, P., Aune, M., Bogstad, B., et al., 2023. Panel-based Assessment of Ecosystem Condition of Norwegian Barents Sea shelf ecosystems. Rapport fra Havforskningen 2023-14, 1893–4536.
Slagstad, D., & Wassmann, P. 1996. Climate change and carbon flux in the Barents Sea: 3-D simulations of ice-distribution, primary production and vertical export of particulate organic carbon. Mem. Natl Inst. Polar Res., 51,119-141,1996.
Slagstad, D., 1984. A model of phytoplankton production in the marginal sea ice zone of the Barents Sea. Model. Identif. Control. 5 (3), 129–140. https://doi.org/10.4173/mic.1984.3.1.
Smedsrud, L.H., Esau, I., Ingvaldsen, R.B., Eldevik, T., Haugan, P.M., Li, C., Sorokina, S. A., 2013. The role of the Barents Sea in the Arctic climate system. Rev. Geophys. 51 (3), 415–449. https://doi.org/10.1002/rog.20017.
Smedsrud, L.H., Muilwijk, M., Brakstad, A., Madonna, E., Lauvset, S.K., Spensberger, C., Årthun, M., 2022. Nordic Seas heat loss, Atlantic inflow, and Arctic sea ice cover over the last century. Rev. Geophys. 60 (1), e2020RG000725 https://doi.org/10.1029/2020RG000725.
Smith, W.H.F., Wessel, P., 1990. Gridding with continuous curvature splines in tension. Geophysics 55, 293. https://doi.org/10.1190/1.1442837.
Stamnes, K., Hamre, B., Stamnes, S., Chen, N., Fan, Y., Li, W., Stamnes, J., 2018. Progress in forward-inverse modeling based on radiative transfer tools for coupled atmosphere-snow/ice-ocean systems: A review and description of the AccuRT model. Appl. Sci. 8 (12), 2682. https://doi.org/10.3390/app8122682.
Strass, V.H., Nothig, E.M., 1996. Seasonal shifts in ice edge phytoplankton blooms in the Barents Sea related to the water column stability. Polar Biol. 16 (6), 409–422.
Sundfjord, A., Assmann, K.M., Lundesgaard, Ø., Renner, A.H.H., Lind, S., Ingvaldsen, R. B., 2020. Suggested water mass definitions for the central and northern Barents Sea, and the adjacent Nansen Basin: Workshop Report. The Nansen Legacy Report Series 8. https://doi.org/10.7557/nlrs.5707.
Tremblay, J.É., Anderson, L.G., Matrai, P., Coupel, P., Bélanger, S., Michel, C., Reigstad, M., 2015. Global and regional drivers of nutrient supply, primary production and CO_2 drawdown in the changing Arctic Ocean. Prog. Oceanogr. 139, 171–196. https://doi.org/10.1016/j.pocean.2015.08.009.
Tschudi, M., Meier, W. N., Stewart, J. S., Fowler, C.. Polar Pathfinder Daily 25 km EASE-Grid Sea Ice Motion Vectors, Version 4 [Data Set]. Boulder, Colorado USA. NASA National Snow and Ice Data Center Distributed Active Archive Center. https://doi.org/10.5067/INAWUWO7QH7B.
[dataset] Vader, A (2022). Chlorophyll a and phaeopigments Nansen Legacy, NMDC. https://doi.org/10.21335/NMDC-1371694848.
von Appen, W.J., Waite, A.M., Bergmann, M., Bienhold, C., Boebel, O., Bracher, A., Boetius, A., 2021. Sea-ice derived meltwater stratification slows the biological carbon pump: results from continuous observations. Nat. Commun. 12 (1) https://doi.org/10.1038/s41467-021-26943-z.
Wassmann, P., Ratkova, T., Andreassen, I., Vernet, M., Pedersen, G., Rey, F., 1999. Spring bloom development in the marginal ice zone and the central Barents Sea. Mar. Ecol. 20 (3–4), 321–346.
Wassmann, P., Reigstad, M., Haug, T., Rudels, B., Carroll, M.L., Hop, H., Pavlova, O., 2006. Food webs and carbon flux in the Barents Sea. Prog. Oceanogr. 71 (2–4), 232–287. https://doi.org/10.1016/j.pocean.2006.10.003.